Atmos. Chem. Phys. Discuss., 9, 10711–10775, 2009
www.atmos-chem-phys-discuss.net/9/10711/2009/

Atmospheric Chemistry and Physics Discussions

This discussion paper is/has been under review for the journal *Atmospheric Chemistry and Physics (ACP)*. Please refer to the corresponding final paper in *ACP* if available.

A new paradigm for intensity modification of tropical cyclones: thermodynamic impact of vertical wind shear on the inflow layer

M. Riemer[1], M. T. Montgomery[1,2], and M. E. Nicholls[3]

[1]Department of Meteorology, Naval Postgraduate School, Monterey, CA, USA
[2]NOAA's Hurricane Research Division, Miami, FL, USA
[3]University of Colorado, Cooperative Institute for Research in Environmental Sciences, Boulder, CO, USA

Received: 16 March 2009 – Accepted: 17 April 2009 – Published: 4 May 2009

Correspondence to: M. Riemer (mriemer@nps.edu)

Published by Copernicus Publications on behalf of the European Geosciences Union.

Abstract

An important roadblock to improved intensity forecasts for tropical cyclones (TCs) is our incomplete understanding of the interaction of a TC with the environmental flow. In this paper we re-visit the classical idealised numerical experiment of tropical cyclones (TCs) in vertical wind shear on an f-plane. We employ a set of simplified model physics – a simple bulk aerodynamic boundary layer scheme and "warm rain" microphysics – to foster better understanding of the dynamics and thermodynamics that govern the modification of TC intensity. A suite of experiments is performed with intense TCs in moderate to strong vertical shear. In all experiments the TC is resilient to shear but significant differences in the intensity evolution occur.

The ventilation of the TC core with dry environmental air at mid-levels and the dilution of the upper-level warm core are two prevailing hypotheses for the adverse effect of vertical shear on storm intensity. Here we propose an alternative and arguably more effective mechanism how cooler and drier (lower θ_e) air – "anti-fuel" for the TC power machine – can enter the core region of the TC. Strong and persistent downdrafts flux low θ_e air from the lower and middle troposphere into the boundary layer, significantly depressing the θ_e values in the storm's inflow layer. Air with lower θ_e values enters the eyewall updrafts, considerably reducing eyewall θ_e values in the azimuthal mean. When viewed from the perspective of an idealised Carnot-cycle heat engine a decrease of storm intensity can thus be expected. Although the Carnot cycle model is – if at all – only valid for stationary and axisymmetric TCs, a strong correlation between the downward transport of low θ_e into the boundary layer and the intensity evolution offers further evidence in support of our hypothesis.

The downdrafts that flush the inflow layer with low θ_e air are associated with a quasi-stationary region of convective activity outside the TC's eyewall. We show evidence that, to zero order, the formation of the convective asymmetry is driven by the balanced dynamical response of the TC vortex to the vertical shear forcing. Thus a close link is provided between the thermodynamic impact in the near-core boundary layer and the

ACPD

9, 10711–10775, 2009

balanced dynamics governing the TC vortex evolution.

1 Introduction

For decades it has been well known that vertical shear of the environmental wind has a detrimental effect on the intensity of tropical cyclones (TCs). The processes that modulate the intensity of a TC when affected by shear, however, are not well understood. This lack of understanding is partially reflected in high uncertainties that still exist in operational TC intensity forecasts. In addition, recent projections of global climate models indicate an increase in vertical wind shear in the tropical North Atlantic (Vecchi and Soden, 2007). Understanding the interaction of TCs and the vertically sheared environmental flow should thus provide not only a significant benefit to the operational forecast community but may also advance our understanding of changes in TC climate characteristics in a globally warming atmosphere.

Numerous previous studies have been devoted to understand the mechanisms by which a TC-like vortex is resilient to vertical shear. For small amplitude vertical shear forcing the differential advection of the vertical shear causes the vortex to tilt and excites vortex Rossby waves (VRWs). Two types of VRW structures have been identified that support the resilience of a TC-like vortex. Propagation of a quasi mode causes the vortex to precess. The exponential decay of this mode leads to vortex alignment. Dispersion and subsequent inviscid damping of sheared VRWs can also lead to the rapid reduction of vortex tilt (Schecter and Montgomery, 2003; Reasor et al., 2004). Moist processes have been shown to significantly enhance the aforementioned adiabatic resiliency mechanisms (Schecter and Montgomery, 2007). The resiliency of TC-like vortices has also been studied in terms of the interaction of lower and upper-level potential vorticity (PV) anomalies (e.g Jones, 1995; Smith et al., 2000) and the impact of diabatic processes on these anomalies (Davis et al., 2008).

While these resiliency studies did not focus on the intensity change of a resilient vortex, it was noted that the excitation of the tilt mode weakens the azimuthal mean cir-

ACPD
9, 10711–10775, 2009

culation of the vortex. During the alignment of the vortex, i.e. the decay of the tilt mode, much of the kinetic energy was fed back into the mean circulation. These changes in the strength of the mean vortex, however, are small (e.g. Reasor and Montgomery, 2001). DeMaria (1996) followed the same idea using PV superposition arguments. Using a 2-layer model he found an intensity decrease of about 10% for a very large vortex tilt (O(100 km)). In contrast, Wong and Chan (2004) found in an idealised numerical experiment a significant intensity decrease with very small tilt. These results suggest that the kinematic effect is not the primary intensity change mechanism.

Wu and Braun (2004) suggested that persistent asymmetries in the TC core that occur due to the interaction with environmental flow weaken the mean circulation by eddy momentum fluxes. Their result was derived from non-cloud-resolving numerical experiments with horizontal grid spacing of 25 km and only considered the kinematic impact of the asymmetries. Very recent work, however, indicates that asymmetries are essential in the intensification process of a TC. Nguyen et al. (2008), performing higher-resolution experiments, identified vortical hot towers (VHTs) as the coherent asymmetric structures in an intensifying TC. The VHTs are locally buoyant and induce near-surface convergence in the boundary layer. For an intensifying TC, Montgomery et al. (2009) found that the vortex-scale density temperature generally lags behind the local density temperature within the VHT cores and thus concluded that these cores are the main driver of the intensification process. We are thus not convinced that the study by Wu and Braun (2004) sufficiently accounts for the role of asymmetries during intensity modification of a TC in vertical shear.

DeMaria (1996) showed, following balance considerations, that a tilted vortex is associated with a warm anomaly at mid-levels leading to a more stable stratification and arguably weaker convection. A reduction of the convective vertical mass flux can be expected to lead to a partial spin down of the lower part of the vortex. Jones (2000), however, demonstrated that the temperature anomalies associated with vortex tilt also *decrease* stability locally and thus might *enhance* convection. It is not clear that the stability anomaly leads to a decrease of convection in the azimuthal average. In fact,

Davis et al. (2008) have shown in 6 model case studies that the vertical mass flux increases with shear magnitude up to shear values of around 15 ms^{-1}.

Emanuel (1986, 1991) proposed an intensity theory for an axisymmetric, steady TC based on thermodynamic arguments. His theory regards the TC as a heat engine, illustrated and further described in Figs. 1a and 2a. The work done by the heat engine is assumed to by converted into kinetic energy that is finally dissipated in the frictional boundary layer. Thus the thermodynamic cycle is linked to the wind field in the boundary layer, i.e. intensity. Some interesting critique has been raised about the thermodynamic reasoning (Makarieva et al., 2008) and the underlying dynamical assumptions (Smith et al., 2008) of this theory. We further note that the closed pathway of air parcels is not realized in our model (neither is it in real storms) and that radiative processes (by which the heat engine is assumed to loose energy at upper-levels) are not represented in our simplified model. We do not intend to use Emanuel's theory in a quantitative manner, but rather only apply its very fundamental idea: that a frustration of the energy cycle yields a decrease in storm intensity.

The development of asymmetries has been invoked to explain observed decrease in intensity. Much attention is given to asymmetries of vertical motion in the eyewall. Earlier studies found a distinct wave number 1 pattern (e.g. Bender, 1997; Frank and Ritchie, 2001) while recent work by Braun et al. (2006) document the internal structure within the wave number 1 envelope. It is, however, not clear why the TC heat engine should not work near peak efficiency in the presence of these asymmetries.

The ventilation of the TC core by dry environmental air at mid-levels (Simpson and Riehl, 1958) was perhaps the earliest idea how TC intensity could be constrained by vertical shear. Mixing of low θ_e air into the eyewall at mid-levels could be particularly effective because the minimum of θ_e is usually located at this level (Fig. 1b). The frustration of eyewall θ_e values would act as a "leak" in the TC engine and reduce its ability to produce work (Fig. 2b). A somewhat similar hypothesis is the dilution of the upper-level warm core by outward fluxes of high θ_e and PV values and the subsequent weakening of the vortex from the top to bottom, invoking hydrostatic arguments (Frank

ACPD
9, 10711–10775, 2009

and Ritchie, 2001). Wong and Chan (2004) expect the dilution of the upper-level core to be enhanced when the shear-forced secondary circulation becomes strong enough to overwhelm the eyewall updrafts. In terms of the TC heat engine, however, the effectiveness of upper-level θ_e mixing is questionable because the radial θ_e gradient is less pronounced. Furthermore, a TC constitutes a strong atmospheric vortex. Air within the vortex tends to be contained and sheltered from intrusion from the environment, in part due to the strong radial shear of the tangential wind. Any asymmetry that tries to invade the vortex tends to be damped by the action of differential shear: this is the so-called vortex axisymmetrisation process (Melander et al., 1987; Carr and Williams, 1989) that is a well known essential ingredient in the robustness and persistence of coherent vortex structures in quasi two-dimensional flows. This aspect has not been explicitly discussed in the studies mentioned above in this paragraph. A trajectory analysis by Cram et al. (2007) in a moderately sheared TC (10–12 ms^{-1}) found a reduction of eyewall θ_e due to environmental entrainment of $O(1)$ K. This small value illustrates the limitation of air parcel exchange between the environment and the eyewall in this case as mid-level θ_e values of the storm environment are typically more than 15 K less than that found in the eyewall of mature storms.

Here we re-visit the classical idealised numerical experiment of a TC in vertical shear (e.g. Bender, 1997; Frank and Ritchie, 2001). In the now standard posing of the problem a TC, after being spun up in quiescent environment, is exposed to a vertical wind shear profile. We intentionally employ a very simple set of physical parameterisations that, as we argue, capture the essence of the TC-shear interaction. A new hypothesis for intensity modification of a TC interacting with vertical shear is proposed and supporting evidence from our experiments presented. The energy cycle is frustrated at its most vulnerable part: the inflow layer of the TC. Strong and persistent downdrafts bring low θ_e air into the boundary layer (BL) of the storm, significantly depressing near-core BL θ_e values (Fig. 1c). Heat fluxes from the warm ocean surface do not recover θ_e values completely, as compared to the undiluted inflow. Air parcels in the eyewall start rising with reduced θ_e values (Fig. 2c). The flushing of the BL with low-θ_e air – anti-fuel

ACPD
9, 10711–10775, 2009

for the TC's engine – is capable of leading to intensity changes of tens of ms^{-1} (and hPa), without the vortex being sheared apart.

The remainder of this paper is organised as follows. Section 2 describes our numerical model, the posing of the problem, and the initial conditions. An overview of the evolution in our experiments is then provided in Sect. 3. The details of the thermodynamic impact on the BL and the structure of the associated downward flux of low θ_e are presented in Sect. 4. Section 5 discusses the formation of the persistent downdrafts and shows evidence that the vortex-scale downdraft distribution is guided by balanced vortex dynamics. In Sect. 6, we comment on the near-core shear evolution and the storm's re-intensification. A discussion of the results and some observational support for our new paradigm is given in Sect. 7 before we present our conclusions in Sect. 8.

2 Experimental setup

2.1 Numerical model formulation

For the numerical experiments we employ the Regional Atmospheric Modeling System (RAMS), developed at Colorado State University (Pielke and Coauthors, 1992; Cotton and Coauthors, 2003). The RAMS is a three-dimensional non-hydrostatic numerical modeling system comprising time-dependent equations for velocity, non-dimensional pressure perturbation, ice-liquid water potential temperature (Tripoli and Cotton, 1981), and mixing ratios of total water and rain. Cloud water and water vapor mixing ratio, and potential temperature are diagnosed.

We use a simple cloud microphysics scheme that is based on the scheme of Kessler (1969) and considers warm cloud processes only. Rain and cloud water may evaporate in unsaturated air. A standard first-order turbulence scheme developed by Smagorinsky (1963) is used for sub-grid-scale mixing, with modifications by Lilly (1962) and Hill (1974) that enhance diffusion in unstable conditions and reduce diffusion in stable conditions. For simplicity, radiative processes are neglected. First, we believe that

ACPD
9, 10711–10775, 2009

they play a minor role only in the evolution of a TC in vertical shear. Further, considerable heat fluxes from the ocean are confined to a relatively small area around the TC, as compared to the size of our computational domain and thus radiative cooling is not needed to balance a negligible warming of the domain during the course of our integration.

The non-hydrostatic RAMS equations are given as follows: the vector momentum equation is

$$\frac{\partial \boldsymbol{v}}{\partial t} = -\boldsymbol{v}\nabla\boldsymbol{v} - \theta_{v0}\nabla\Pi' + f\boldsymbol{v}\times\boldsymbol{k} - g\left[\frac{\theta'_v}{\theta_{v0}}(r_t - r_v)\right]\boldsymbol{k} + \nabla(K_m\nabla\boldsymbol{v}). \quad (1)$$

The thermodynamic equation is

$$\frac{\partial \theta_{il}}{\partial t} = -\boldsymbol{v}\nabla\theta_{il} + \nabla(K_h\nabla\theta_{il}). \quad (2)$$

The water species mixing ratio equations are

$$\frac{\partial r_n}{\partial t} = -\boldsymbol{v}\nabla r_n + \nabla(K_h\nabla r_n) + S. \quad (3)$$

The mass continuity equation is

$$\frac{\partial \Pi'}{\partial t} = -\frac{R\Pi_0}{c_v\rho_0\theta_{v0}}\left[\nabla(\rho_0\theta_{v0}\boldsymbol{v})\right]. \quad (4)$$

Here $\boldsymbol{v}$ is the three-dimensional velocity vector, θ is potential temperature, the Exner function

$$\Pi = c_p\left(\frac{p}{p_r}\right)^{\frac{R}{c_p}}, \quad (5)$$

with total pressure p, the reference pressure p_r=1000 hPa, R is the gas constant for dry air, c_p the specific heat capacity for dry air at constant pressure, f the Coriolis parameter, θ_v is virtual potential temperature, r_t the total water mixing ratio, r_v the vapor

ACPD
9, 10711–10775, 2009

mixing ratio, K_m and K_h the eddy viscosity coefficient for momentum and enthalpy, respectively, θ_{il} the ice-liquid water potential temperature (as we do not consider the ice phase, θ_{il} reduces to liquid water potential temperature, see Eq. 6), r_n represents mixing ratios of total water (r_t) and rain (r_r), S a source/sink term from conversion of water species and precipitation, c_v the specific heat capacity for dry air at constant volume and ρ is air density. Thermodynamic variables are decomposed into a horizontal reference state (denoted by subscript zero) from which the predicted deviations (denoted by a prime) should be small. To represent the interaction between the model atmosphere and the underlying sea surface the momentum and thermodynamic equations (Eqs. 1 and 2, respectively) are further modified by surface fluxes as discussed below.

The potential temperature is diagnosed as:

$$\theta = \theta_{il}\left[1 + \frac{L_{lv} r_l}{c_p \max(T, 253)}\right]. \quad (6)$$

The mixing ratio of liquid water $r_l = r_c + r_r$ (where r_c is the cloud water mixing ratio) and L_{lv} is the latent heat of condensation. Water vapor is diagnosed from

$$r_v = r_t - r_r - r_c \quad (7)$$

and cloud water from

$$r_c = \max(r_t - r_r - r_{\text{vsat}}, 0) \quad (8)$$

where the saturation mixing ratio is given by

$$r_{\text{vsat}} = \frac{0.622 e_{sv}}{p - e_{sv}}. \quad (9)$$

The saturated vapor pressure e_{sv} is a function of temperature T and calculated from Clausius-Clapeyrons equation. Finally, temperature is diagnosed from

$$T = \frac{\theta \Pi}{c_p}. \quad (10)$$

ACPD
9, 10711–10775, 2009

Equations (6–10) are solved iteratively.

Cloud water is assumed to move with the air while rain is also allowed to sink relative to the air. The terminal velocity increases as a power of the droplet diameter and is based on empirical data. In the absence of rain, cloud water forms as soon as saturation is exceeded (Eq. 8). Clouds form on a prescribed distribution of cloud condensation nuclei. An autoconversion parameterisation that depends on the cloud water mixing ratio and the mean diameter of the cloud droplets is used to represent the formation of rain by collision and coalescence of cloud droplets.

2.2 Grid configuration

RAMS utilises the two-way interactive multiple nested grid scheme developed by Clark and Farley (1984). This allows explicit representation of cloud-scale features within the finest grid while enabling a large domain size to be used, thereby minimizing the impact of lateral boundary conditions. A standard radiation boundary condition is used at the lateral boundaries, which assumes that disturbances reaching the boundary move as linearly propagating gravity waves (Klemp and Wilhelmson, 1978). A Rayleigh friction layer is included at upper-levels (above 17 km) to minimize the reflection of gravity waves from the top of the model. At the lower boundary the vertical velocity is required to vanish.

2.3 Surface interaction

The bulk aerodynamic formulas are used to calculate the momentum and heat fluxes from the sea surface. The fluxes are calculated as

$$\overline{w'u'} = -C_D|V|_1 u_1 \tag{11}$$

$$\overline{w'v'} = -C_D|V|_1 v_1 \tag{12}$$

$$\overline{w'\theta'} = -C_K|V|_1(\theta_1 - \theta_s) \tag{13}$$

ACPD
9, 10711–10775, 2009

$$\overline{w'r'} = -C_K|V|_1(\theta_1 - \theta_s). \quad (14)$$

The subscripts $_1$ and $_s$ denote values at the lowest model level and at the surface, respectively, and $|V|$ denotes the horizontal wind speed. The drag coefficient is represented by Deacons formula:

$$C_D = 1.1 \times 10^{-3} + 4 \times 10^{-5}|V|_1. \quad (15)$$

C_K is the exchange coefficient of enthalpy with the ratio

$$\frac{C_K}{C_D} = 1. \quad (16)$$

The latest findings on the dependence of these exchange coefficients on wind speed (Black et al., 2007; Zhang et al., 2008) indicate that, in particular for high wind speeds, $\frac{C_K}{C_D}$<1. These new results should be incorporated in future tests of our findings with respect to uncertainties in the model parameterisations. Here we speculate that a decrease of C_K in the higher wind regime would actually emphasise the importance of our proposed mechanism: depressed BL θ_e values would be replenished more slowly and their effect on the eyewall updrafts, and thus intensity, would be more pronounced.

2.4 Domain setup and initial conditions

We use 3 domains with a horizontal grid spacing of 45 km, 15 km and 5 km, respectively. The outermost domain contains 120×120 grid points giving a domain size of 5400×5400 km. The second and third domains have 200×122 (3000×1830 km) and 400×160 (2000×800 km) grid points, respectively. Both inner grids are centered within the outermost domain. We use 38 vertical levels with the lowest level at 49 m. The vertical resolution is 100 m between the lowest two levels and decreases with height by a stretching factor of 1.09 between grid levels. The top of the model resides at 24.6 km. The model domain is on an f-plane and the Coriolis parameter valid for 15° N. A modified Jordan sounding (Jordan, 1958) is used as the background sounding. While the

ACPD
9, 10711–10775, 2009

temperature profile is retained the low-level moisture is reduced with a maximum drying of 2 gkg^{-1} at the surface. The low-level drying is employed to retard convective activity not associated with the TC. The time-invariant SST is set to 28.5°C.

The initial vortex has an axisymmetric structure with a maximum wind speed of 20 ms^{-1} at radius 135 km and 4 km height. The maximum surface wind speed is 18 ms^{-1} and the vortex has a depth of 10 km. For a radius less than 75 km the vortex is moistened to 90% of saturation. Between a radius of 75 to 100 km the moisture anomaly is linearly reduced to zero. The initial vortex is centered in the fine grid in the meridional direction. In anticipation of a predominantly westward movement in the shear experiments, the vortex is initially placed in the eastern part of the innermost nest, 250 km away from the transition to grid 2.

2.5 Vertical shear profile in thermal wind balance

For the shear experiments we superimpose a wind field in thermal wind balance after the vortex spin up phase. The shear profile is given by a cosine structure:

$$U(z) = U_m \left[1 - \cos\left(\frac{\pi z}{H}\right)\right] \text{ for } z \le H, \tag{17}$$

$$U(z) = 2U_m \text{ for } z > H. \tag{18}$$

The associated temperature and pressure perturbations in thermal wind balance with the shear profile are given by

$$\theta'_v(y,z) = \theta_{v0}\frac{fy}{g}U_m\left[\frac{1}{\theta_{v0}}\frac{d\theta_{v0}}{dz} - \frac{\pi}{H}\sin\left(\frac{\pi z}{H}\right) - \cos\left(\frac{\pi z}{H}\right)\frac{1}{\theta_{v0}}\frac{d\theta_{v0}}{dz}\right] \tag{19}$$

$$\Pi'(y,z) = -\frac{fy}{\theta_{v0}}U_m\left[1 - \cos\left(\frac{\pi z}{H}\right)\right] \tag{20}$$

below z=H and by

$$\theta'_v = -\frac{f}{g}2U_m\frac{d\theta_{v0}}{dz}y \tag{21}$$

ACPD
9, 10711–10775, 2009

$$\Pi' = \frac{f}{\theta_{v0}} 2U_m y \tag{22}$$

above. We use 12 km as the height H of maximum wind $2U_m$. The velocity change between the surface and 12 km height is thus given by $2U_m$. For our shear profile this corresponds approximately to the commonly used shear value between 850 hPa to 200 hPa. Here we conduct experiments with $2U_m$ values of 0, −10, −15, and −20 ms^{-1}; these experiments will hereafter be referred to as no_shear, 10mps, 15mps, and 20mps case, respectively. The negative values denote easterly shear. Note that this profile exhibits zero surface wind and shear.

A slight imbalance occurs when superposing the balanced field on the tropical cyclone after the spin up phase. We do not see any indication that this imbalance compromises our experiment or subsequent physical interpretations after the short adjustment time to the imposed shear.

3 Overview of storm evolution

In this section we give an overview of the simulated TC evolution in terms of intensity, track, and vortex tilt in the respective experiments.

The intensity measure in this study is the maximum azimuthal average of the tangential wind in 1 km height. The center of the storm is calculated iteratively as the centroid of positive relative vorticity in a 120 km×120 km box around the center, averaged over the lowest 2 km. The surface pressure minimum is used as the initial first guess center of the square. The center of the square is adjusted and the vorticity centroid recalculated if the centroid differs more than half a grid length from the previous one. Data from the innermost nest is used and the centroid calculation usually converges after 2–3 steps. The tilt of the vortex is calculated as the difference between the position vectors of the vorticity centroid at 10 km and 1 km height.

ACPD
9, 10711–10775, 2009

3.1 Spin up period and evolution without environmental shear

In the first 20 h the initial vortex intensifies rapidly to 50 ms^{-1} (Fig. 3). In the next 20 h the storm continues to intensify at a much slower rate. A second period of rapid intensification follows in which the TC intensifies to 80 ms^{-1} at 60 h. The storm continues to intensify gradually and reaches a quasi-steady intensity of about 95 ms^{-1}–100 ms^{-1} after 84 h. As in previous studies, the environmental wind profile in the shear experiments is superimposed at 48 h. We note that this is during a time of rapid intensification. In the following we only consider the time period after the shear is imposed, i.e. the time after 48 h. We hereafter refer to this time as time 0 h.

To illustrate the vortex structure at 0 h the azimuthally averaged radial profiles of tangential wind at 1 km and vorticity above the BL at 2 km height are depicted in Fig. 4 (solid lines). The vorticity distribution has a bowl-shaped structure in the inner core and the radial gradient changes its sign at ≈20 km radius. The vorticity profile thus allows for barotropic instability. It has been suggested (e.g. Schubert et al., 1999) that mixing of vorticity and also θ_e in the inner core can lead to TC intensity changes. In the sheared cases the vorticity profile predominantly shows a monopole structure soon (2–4 h) after the shear is imposed (exemplified for the 20mps case by the thin dashed line in Fig. 4). This is consistent with vorticity mixing in the inner core early in the shear experiments. The intensity modification, however, is minor during this mixing period and actually the storm slightly intensifies (thick dashed line in Fig. 4). The decrease in intensity associated with vertical shear is found on a much longer time scale of 12–24 h (see below). We are thus confident that vorticity mixing processes in the inner core region are not a major component of the significant intensity modification in our experiments. The vorticity and wind profiles after the initial weakening are exemplified in Fig. 4 by the dotted lines.

After the spin up period the vortex tilt in the no_shear case is below 5 km expect for two peaks at 3 h (10 km) and 18 h (8 km) (Fig. 5). The tilt direction indicates a

ACPD
9, 10711–10775, 2009

high-frequency internal precession mode of 3–4 h[1] (not shown). These intrinsic tilt characteristics are the benchmark against which the tilt evolution in the sheared cases will be compared.

3.2 Shear cases

3.2.1 Storm movement

The vertical shear profile implies a steering flow for the TC. The TCs move with an average speed of 3.5 ms^{-1}, 5 ms^{-1}, and 6.5 ms^{-1} in the 10mps, 15mps, and 20mps case, respectively. The storm tracks within the innermost domain are depicted in Fig. 6. In the 20mps case, the TC center approaches the western boundary closely and the experiment is stopped at 69 h. The tracks of the storms have a southward component, likely due to a combination of the downshear displacement of the outflow anticyclone (see also Sect. 6) and the "β-drift" on the gradient of potential vorticity associated with the environmental shear flow.

3.2.2 Intensity evolution and storm resiliency

An imposition of moderate to strong shear hinders the rapid intensification[2] (10mps case) or leads to an intensity decrease (15mps and 20mps cases, Fig. 3). In all of these cases, the simulated storms re-intensify after a period of weakening. We offer further comments on the recovery of the storms in Sect. 6. In the 10mps and 15mps cases the intensity reaches maximum values only slightly ($\approx$5 ms^{-1}) less than in the no_shear case. In the 20mps case the maximum intensity at the end of the experiment is significantly (20 ms^{-1}) less than in the no_shear case.

[1]The precession frequency is estimated from hourly data of the tilt direction. It is possible that the true precession frequency is not resolved due to insufficient temporal sampling.

[2]The suspension of intensification constitutes a weakening relative to the no_shear case and will thus be referred to as weakening in the following.

ACPD
9, 10711–10775, 2009

Using the azimuthal mean tangential wind speed at 1 km height as the intensity metric, the TC intensity decreases with higher shear values. A more complex intensity behavior is found in terms of the maximum local wind speed at 1 km height. Using this measure the most intense storm is found in our 15 ms^{-1} shear experiment, 10 ms^{-1} stronger than the no shear case at the end of the experiment (not shown). The location and evolution of the local wind maxima in sheared TCs have, of course, considerable implications at landfall and possibly for the generation of storm surge and are thus important subjects for future research.

Although other studies have found TCs to decay at smaller values of vertical shear (e.g Frank and Ritchie, 2001), the resiliency of the vortex in the higher shear regime is not a unique feature of our experiments. Wang et al. (2004) found resilient TCs for shear values up to 17 ms^{-1} in a very similar experimental setup. In a simulation of Erin by Braun and Wu (2007) the model TC did not decay in a shear environment of 20 ms^{-1} (the authors noted that the shear in their simulation was greater than in reality). In a simulation of Hurricane Bonnie (Braun et al., 2006) the hurricane intensified in 10–12 ms^{-1} shear. There is also observational evidence (e.g Black et al., 2002, Hurricane Jimena in 13–20 ms^{-1} shear) that TCs can remain intact in strong shear. We are thus confident that the resiliency of the TC is not a pathology of our numerical model or the employed parameterisations.

The vortex tilt in the shear experiments is significantly larger than in the no_shear case in the early evolution (Fig. 5). As can be expected, the vortex tilt increases with the magnitude of the shear. Later in the evolution, the tilt magnitude decreases in all experiments. After 24 h the tilt is about 5 km in the 10mps and 15mps cases, only slightly larger than in the no shear case. In the 20mps case it takes longer (about 36 h) for the vortex to reduce the tilt. Subsequently, tilt values larger than 10 km can still be found. For all cases, however, it is evident that the vortices are resilient to the detrimental effect of the shear and tend to re-align in the course of the experiment. The tilt evolution will be discussed further in Sect. 5.

ACPD
9, 10711–10775, 2009

4 Thermodynamic impact of vertical shear on the boundary layer

It will be shown in this section that the interaction with vertical shear has a profound impact on the thermodynamic structure of the BL. Downdrafts transport low θ_e air into the BL and form extended areas of depressed BL entropy, ultimately leading to a reduction of θ_e values within the eyewall updrafts. We will argue that this constitutes a frustration of the TC's energy cycle. The structure, magnitude, and evolution of the depressed BL θ_e will be documented and its impact on the azimuthal mean structure of the storm quantified. We will calculate the downward flux of low θ_e air into the BL and show that this downward flux is highly correlated with the intensity evolution.

4.1 Near-core entropy modification in the boundary layer

4.1.1 Banded structure of significantly reduced θ_e

An extensive region of considerably reduced BL θ_e values can be found within a few hours after the vertical shear is imposed. This region of depressed BL θ_e forms a quasi-stationary band that spirals inward from the Northwest and approaches the eyewall on the upshear side (East) of the storm (Fig. 7). The band can extend outwards up to 150–200 km radius. The θ_e depression is significant, with values of BL θ_e 15–20 K lower than in the no_shear case. The low θ_e values first appear to the Southwest of the storm center (not shown). For higher shear values the low θ_e air covers a larger area, in particular close to the eyewall South and East of the center (downshear-left and upshear).

In the 10mps case this spiral pattern lasts until 6 h and reappears from 14 h to 18 h. In the 15mps and 20mps case the spiral pattern becomes somewhat less distinct after 7 h but low θ_e values still dominate the BL in the near-core region until 24 h and 36 h, respectively. This extensive region of depressed BL θ_e is associated with the pronounced intensity decrease after imposing the shear (cf. Fig. 3).

In the no_shear case there is an indication of a spiral pattern of depressed θ_e values

ACPD
9, 10711–10775, 2009

also (Fig. 7a). Besides being far less pronounced, this spiral does not reach close to the eyewall and is a transient feature.

4.1.2 Recovery of boundary layer θ_e

The BL θ_e values recover after the widespread initial depression. The recovery process is illustrated for the 15mps and 20mps case in Fig. 8 by displaying two representative BL θ_e configurations, respectively. At 32 h the BL θ_e values have recovered to a large degree in the 15mps case (Fig. 8a). Less pronounced bands of lower θ_e air (exemplified in Fig. 8b) infrequently interrupt the recovery process. The BL recovery in the 20mps case is much less complete. The BL θ_e pattern rarely has a symmetric appearance, an exception is depicted in Fig. 8c. A band of low θ_e air spiraling towards the eyewall is found much more frequently (Fig. 8d), reminiscent of the initial pattern depicted in (Fig. 7d) but less pronounced. A more complete recovery is found only after 60 h (not shown). The slow and incomplete recovery of BL θ_e values in the 20mps case is consistent with the lower intensity and the delayed re-intensification of the storm. In the 10mps case the BL θ_e values have almost completely recovered at 20 h (not shown), consistent with the early re-intensification of the storm. Subsequently, confined areas of low BL θ_e values are found infrequently only.

4.1.3 A link to the convective asymmetry outside of the eyewall

The BL θ_e evolution is associated with a pronounced convective asymmetry outside of the eyewall. At early times in the shear experiments strong convective activity is found downshear-right of the center (Fig. 7). The convection takes the form of bands and clusters that tend to rotate from the downshear-right into the downshear quadrant. This convective asymmetry is, in general, well pronounced until 30 h in the 15mps case. With the demise of the convective asymmetry the BL θ_e starts to recover (Fig. 8a). Subsequently, the convective asymmetry occurs infrequently only, usually associated with somewhat lower BL θ_e values (e.g. Fig. 8b). In the 20mps case the pronounced

ACPD
9, 10711–10775, 2009

convective asymmetry prevails until 60 h (e.g. Fig. 8b), interrupted by a short period of more axisymmetric structure around 46 h (Fig. 8c). Again, the more axisymmetric distribution of convection outside the eyewall is associated with a short period of recovered BL θ_e values. A minimum in the convective asymmetry in the 10mps case is found around 12 h with a re-establishment of the structure shown in Fig. 7b afterwards (not shown). After 24 h, a pronounced and quasi-stationary asymmetry is no longer found.

In all of our experiments, a depression of BL θ_e in general occurs in association with a quasi-stationary convective asymmetry outside of the eyewall. Section 5 will discuss the generation and the importance of this convective asymmetry in further detail.

4.1.4 Impact on the azimuthal mean structure

The BL θ_e depression is clearly an asymmetric feature with a strong wave number 1 structure. A theory for TC intensity, however, only exists for axisymmetric storms. We note that an axisymmetric theory might be an oversimplification for a strongly asymmetric TC. Further progress needs to be made in our theoretical understanding of intensity evolution of asymmetric storms to tackle the important forecast problem of vertical shear impacts on storm intensity. Lacking a more complete theoretical foundation we present the axisymmetric approach in this publication and address the importance of the pronounced wave number 1 asymmetries to intensity modification in future work.

To interpret our results in the framework of the thermodynamic cycle illustrated in Fig. 1a we first consider the impact of the observed pattern of BL θ_e depression on the azimuthal mean structure of the storm. Figure 9 depicts the vertical and radial distribution of θ_e in the lower part of the TC at the same early time as in Fig. 7. The same general structure is found in all shear cases: a tongue of low θ_e air intrudes into the BL and radially inward towards the eyewall updrafts. The θ_e depression is most pronounced between 50 km and 100 km radius. As can be expected from the horizontal plots in Fig. 7 the tongue of low θ_e is more pronounced for higher shear values. A similar structure of the azimuthally averaged θ_e distribution is also found at

ACPD
9, 10711–10775, 2009

subsequent times when bands of decreased BL θ_e values are present (e.g. at the times depicted in Figs. 8b and 8d, vertical cross sections not shown). The intrusion of low θ_e air at these times is somewhat less pronounced and confined closer to the eyewall.

We estimate a representative θ_e value of air rising in the eyewall by visually averaging the θ_e values within the $1\,\mathrm{ms}^{-1}$ updrafts in Fig. 9. Compared to the no_shear case we find lower θ_e values of 9 K, 4 K, and 3 K in the 20mps, 15mps, and 10mps case, respectively. The reduction of eyewall θ_e at this time clearly precedes the distinct subsequent intensity evolution: Under no-shear conditions the storm intensifies in the following 12 h to $87\,\mathrm{ms}^{-1}$, the intensification in the 10mps case is significantly less and the TCs in the 15mps and 20mps cases both weaken (cf. Fig. 3).

A trajectory analysis of Cram et al. (2007) found a decrease of eyewall θ_e by entrainment of environmental air at mid-levels of $O(1)$ K in a full physics model simulation of a mature, moderately sheared ($12\,\mathrm{ms}^{-1}$) hurricane. A comparison with the values above suggest that BL processes dominate the intensity evolution in our numerical experiment and that mid- and upper level processes are of secondary importance only.

The radial profile of the azimuthal mean tangential winds at 2 km (the upper bound in Fig. 9) is very similar in all cases, while the wind maximum between 500 m and 1 km has already decreased by 7 and $15\,\mathrm{ms}^{-1}$ in the 15mps and 20mps case, respectively. The vortex apparently weakens at lowest levels first. This notion further supports our hypothesis that low-level processes – the depression of BL entropy by shear-induced downdrafts – govern the intensity evolution in our experiment.

4.2 Downward flux of low θ_e air into the boundary layer

The vertical structure of the azimuthal mean θ_e field as well as the temporal evolution of the asymmetric BL θ_e depression offer evidence that low θ_e air is brought into the BL from above[3]. This downward import is now examined in more detail.

[3]Non-pseudoadiabatic processes, e.g. precipitative flux, are arguably of secondary importance for the depression of BL θ_e values.

ACPD
9, 10711–10775, 2009

4.2.1 A definition of downward flux

Here we define the downward flux θ_e at the top of the BL as

$$\mathrm{DFX} \equiv w\_\theta'_e, \tag{23}$$

where $w\_$ is negative vertical motion and the prime denotes the deviation from the azimuthal mean. The top of the BL is defined as 1.5 km, roughly the top of the axisymmetric inflow layer. Positive values of DFX denote downward flux of low θ_e into the BL. The definition of DFX differs from the vertical eddy flux of θ_e ($w'\theta'_e$) in that the latter expression yields positive values for upward flux of high θ_e anomalies out of the BL also. Downward flux of low θ'_e and upward flux of high θ'_e can therefore not be distinguished. Definition 23 is also somewhat different from $w'\_\theta'_e$. In the latter expression upward motion that is smaller than the azimuthal mean indicates downward flux of low θ_e also. The horizontal distributions of $w'\_\theta'_e$ and DFX are similar (not shown). The azimuthal mean of $w'\_\theta'_e$ ($\overline{w'\_\theta'_e}$) differs from $\overline{\mathrm{DFX}}$ only by the additional term $\overline{w'_+\theta'_e}$ where $(|w'_+|)<(|\overline{w\_}|)$. As $\overline{w\_}$ is usually found to be very small ($O(1\ \mathrm{cms}^{-1})$) the azimuthal averages $\overline{\mathrm{DFX}}$ and $\overline{w'\_\theta'_e}$ are virtually the same. As we are interested in air parcels that indeed penetrate into the BL from above we hereafter use DFX (Eq. 23).

4.2.2 Downward flux pattern and evolution

The downward flux DFX, averaged over the first 6 h of shear, is shown in Fig. 10. At this early time the downward flux pattern matches very well the structure of low θ_e values in the BL. Downward flux of low θ_e air is found in a banded region extending from ≈200 km radius West (downshear) of the center to close to the eyewall on the East (upshear) side. The downward flux of low θ_e is more pronounced for stronger shear values. Comparing Figs. 7 and 10 it is clearly evident that low BL θ_e air is advected by the swirling winds also, in particular in the 15mps and 20mps case, extending the area of depressed BL entropy into the northeastern quadrant of the storm.

ACPD
9, 10711–10775, 2009

After 5 h, a characteristic value of the θ_e depression in the 15mps case is 15 K at 60 km radius. Assuming an azimuthal wind of 50 ms^{-1} an air parcel circumvents the center at this radius in ≈2 h. Significant DFX values are found approximately in a semicircle around the center. A BL air parcel thus remains in an area of downward flux of low θ_e for ≈1 h. For the 15mps case we estimate an average DFX value of 3 K ms^{-1}. To cool a BL column of 1 km by 15 K it thus takes ≈1.5 h. This short time scale, in particular as we have neglected the replenishment of θ_e by surface fluxes, is consistent with the occurrence of the BL θ_e depression soon after the shear is imposed. This estimate and the spatial patterns shown in Figs. 7 and 10 offer strong evidence that the BL θ_e depression is caused by downward flux of low θ_e air into the BL.

The instantaneous DFX distribution for the 15mps case is illustrated in Fig. 11. The instantaneous field exhibits a pronounced quasi-stationary banded structure in the first ≈24 h after the shear is imposed (exemplified in Fig. 11a), however with a notable variability in magnitude. The orientation of the band slightly shifts counterclockwise (not shown), extending southwest to northeast, consistent with the gradual increase of the northerly shear component (see Sect. 6). From 24–48 h the DFX pattern is less distinct and a pronounced band of downward fluxes occurs infrequently only. After 48 h the downward flux is found to occur predominantly on the upshear side of the storm, adjacent to the eyewall (Fig. 11b). The 10mps case shows very similar characteristics, albeit with smaller magnitude (not shown). In the 20mps case the banded structure dominates until ≈48 h and subsequently, pronounced bands still occur frequently (not shown).

In the no_shear case bands of downward flux of low θ_e are also indicated frequently. However, these bands are of smaller radial extent, the magnitude of downward transport is much less and, in particular, they rotate around the vortex and thus do not exhibit the quasi-steady location as their counterparts in the sheared cases do. The largest values of downward flux in the no_shear case are in general found adjacent to the eyewall. An example of the transient nature of the DFX pattern in the no_shear case is given in Fig. 12.

ACPD
9, 10711–10775, 2009

The sudden introduction of shear constitutes an artificial impact on the TC. The θ_e fluxes, however, show coherent temporal and spatial structure in the shear experiment's. We thus believe that imposing the shear in an instantaneous – and thus rather unrealistic – manner should not invalidate the use of our model results for the real atmosphere.

4.3 Intensity modification and θ_e flux

Consistent with our examination of the azimuthal mean θ_e structure we now consider the azimuthally averaged downward flux of θ_e, $\overline{\mathrm{DFX}}$. For the azimuthal average we can examine the time evolution of the magnitude and the radial distribution of the θ_e flux in a compact manner and compare it with the intensity evolution (Fig. 13).

Inspection of Fig. 13 shows that the overall magnitude of the downward flux increases with higher shear values. In the no_shear case (Fig. 13a) the downward flux of low θ_e air is mostly confined to within 80 km of the storm center. It is interesting to note that the downward flux of low θ_e air near the eyewall becomes a persistent feature after the storm has reached its quasi-equilibrium intensity of 100 ms^{-1} at ≈45 h. In the shear experiments not only the magnitude of the downward flux is greater but the radial extent is larger than in the no_shear case also. Bands of downward flux frequently extend out to a radius of 140 km–150 km. A much larger area of the BL is thus affected by downward flux of low θ_e in the shear cases. The largest values are found outside the radius of maximum winds (RMW) between 40 km and 80 km radius. Considerably smaller values can also be found within the RMW.

The initial weakening in the shear cases is clearly associated with enhanced low θ_e flux into the BL. This initial flushing of the BL with low θ_e air lasts for about 6 h, 12 h, and 24 h in the 10mps, 15mps, and 20mps case, respectively. After this initial period, there is a high correlation between the intensity evolution and $\overline{\mathrm{DFX}}$ on the time scale of a few hours. Periods of re-intensification are usually associated with weak fluxes, whereas strong fluxes most often precede periods of weakening or an interruption in re-

ACPD
9, 10711–10775, 2009

intensification. We have highlighted some illustrative flux events with light gray arrows in Fig. 13. In the 10mps case (Fig. 13b) there is a clear correlation between $\overline{\mathrm{DFX}}$ and intensity at 13 h, 35 h, 45 h, and 68 h. In the 15mps case (Fig. 13c) the flux events at 19 h and 26 h frustrate the re-intensification of the storm. During the subsequent period of relatively small values of $\overline{\mathrm{DFX}}$, intensity increases from 75 ms^{-1} to 90 ms^{-1}. A local intensity minimum around 40 h is associated with enhanced downward flux. The storm does not intensify above 90 ms^{-1} before a period of small $\overline{\mathrm{DFX}}$ values starts at 53 h. The 7 ms^{-1} weakening late in the experiment can be attributed to a flux maximum at 65 h. In the 20mps case (Fig. 13d) periods of strong fluxes of low θ_e air into the BL frustrate the re-intensification of the storm around 28 h, 40 h, 48 h, 53 h, 59 h, and 63 h. In the no_shear case maxima in $\overline{\mathrm{DFX}}$ at 18 h and 33 h precede distinct local minima in intensity.

The high correlation of downward flux of low θ_e air into the BL and the intensity evolution is evidence that the depression of the near-core BL θ_e plays a significant role in the intensity modification of the sheared TC. The radial-height cross sections (Fig. 9) have demonstrated that, arguably by the radial advection in the inflow layer, the lower BL θ_e values outside the eyewall lead to a significant decrease of θ_e in the eyewall updrafts also. A significant impact of shear pertinent to intensity modification is thus a frustration of the energy cycle of the storm in the inflow layer. An axisymmetric intensity theory, however, is not satisfying in the presence of the pronounced wave number 1 asymmetry, and future work should be directed to better understand the contribution of inner core asymmetries in intensity modification.

5 Dynamical origin of the boundary layer θ_e depression

In the previous section, we have presented evidence that the intensity modification of our sheared TCs is tied to the depression of the near-core BL θ_e caused by downward flux of low θ_e air. We will now show that the downward flux is due to downdrafts

ACPD
9, 10711–10775, 2009

associated with a quasi-stationary convective asymmetry outside of the eyewall. This convective asymmetry, as we will argue, has its origin in the asymmetric balanced dynamics of the TC.

Only a brief assessment of the vortex dynamics is given here but a detailed investigation is presented in a subsequent paper. The upshot of this is that the tilt of the sheared TCs in our full physics experiments, including the tilt of the outer vortex at larger radii, can be approximated to zero order by a standing wave number 1 VRW pattern.

Our focus here will be on the 15mps case. The features to be discussed have essentially the same characteristics in the 10mps and 20mps case.

5.1 Is response to shear forcing dominated by balanced dynamics?

The response to vertical shear of an initially barotropic and dry vortex can be explained in terms of VRW dynamics (Reasor et al., 2004). The perturbation of a vortex by shear strongly projects onto a vertical and azimuthal wave number 1 VRW. Reasor et al. have shown that, for a shear profile matching the vertical wave number 1 perturbation, the vortex dynamics can be described as a forced-damped oscillation. The quasi-equilibrium solution for the tilt direction is left of the shear vector and the tilt magnitude decays slowly in time. Schecter and Montgomery (2007) have presented an alpha model for including the principal effects of moist processes on VRWs. This model predicts that cloud coverage will significantly increase the damping rate and thus increase the resiliency of the vortex. The theory has not yet been extended to account for the secondary circulation of a TC.

The TC in our experiment exhibits baroclinic structure and a pronounced secondary circulation, and unbalanced motion is fully accounted for in the numerical model. Despite these complexities, it is remarkable that the tilt evolution of the sheared TC in our experiment is consistent with the predictions of the dry, balanced theory of Reasor et al., as we will demonstrate below.

5.1.1 Some details on the tilt evolution of the modeled TC

As discussed in Sect. 3, all of the sheared TCs in our experiment are resilient and reduce their tilt with time. We now revisit the tilt evolution and consider the tilt direction also. The tilt rapidly settles in a southern direction and only small oscillations around this equilibrium direction appear in the first 18 h (Fig. 14). While the tilt direction stays in the equilibrium direction, the tilt magnitude decreases slowly in time (Fig. 5), qualitatively consistent with the prediction of the forced-damped harmonic oscillator model of Reasor et al.. The decrease of vortex tilt during this time can thus be regarded as the manifestation of inviscid VRW damping of the tilt mode. A comparison of vertical cross-sections of the total vorticity field and the azimuthal wave number 1 field along the tilt axis suggests that indeed much of the total tilt structure is captured by wave number 1 (not shown). After the tilt magnitude has decreased significantly around 18 h the oscillation of the vortex starts to deviate from the equilibrium direction. A higher frequency precession is then indicated in Fig. 14. The precession frequency is in the range of the precession frequency of the vortex in the no_shear case (see Sect. 3.1). The tilt magnitude after 18 h is only slightly greater than in the no_shear case.

5.1.2 The guiding hand of wave number 1 asymmetries

Using a Fourier analysis, we have confirmed that wave number 1 is by far (65–90%, not shown) the dominant contribution to the total asymmetry of the tangential wind and the pressure fields[4]. The horizontal structure above the BL is well represented by wave number 1 (not shown). The ratio of the wave number 1 perturbation and the azimuthal mean is small (0.05–0.2, not shown).

The power spectra of vorticity and vertical motion are significantly flatter than for pressure and horizontal winds (not shown). This can be expected as both fields are

[4]The values for the radial wind are essentially the same but the perturbation is not small compared to the azimuthal mean of the radial velocity.

ACPD
9, 10711–10775, 2009

highly coupled to convective processes that occur preferably at smaller scales. For both fields the wave number 1 asymmetry is not small compared to the respective azimuthal mean field. The wave number 1 pattern of the fields, however, forms an envelope in which most of the smaller scale asymmetries reside. This notion is illustrated for the vorticity field at a representative time in Fig. 15a.

5.1.3 A preliminary balance assessment

The dominance of the wave number 1 pattern implies, in terms of asymmetric balance (AB) theory (Shapiro and Montgomery, 1993), a balanced nature of the asymmetric structure. For nearly steady flow asymmetries the AB expansion parameter is defined in the sense of a local Rossby number for azimuthal wave number n,

$$R_l^2 = \frac{n^2\overline{v}^2/r^2}{\overline{\eta}\overline{\xi}}, \tag{24}$$

with the mean tangential velocity $\overline{v}$, radius r, mean absolute vorticity $\overline{\eta}$, the local Coriolis parameter $\xi = f + 2v/r$, and the standard Coriolis parameter f. For n=1 the local Rossby number is less than unity out to 50 km radius and exceeds unity only in localized regions at larger radii (not shown). The balanced model is used with the general understanding that the balanced nature of the flow may extend somewhat beyond the formal validity of the model. Further, we do not attempt to use the model in a quantitative, predictive sense, but rather to gain a basic, qualitative understanding of the nature of the asymmetries.

The relation of the vorticity and the pressure perturbations further supports the balanced nature of the wave number 1 asymmetries. The maxima in pressure and vorticity perturbation within the eyewall anti-correlate (low ~ cyclonic) very well (not shown). As would be expected for a quasi-balanced flow with its corresponding elliptic inversion operator, the large vorticity perturbations in the near-core region also dominate the pressure perturbation further outside. Inverting the vorticity (PV) field to recover the

ACPD
9, 10711–10775, 2009

pressure distribution would be more stringent evidence of the balanced nature, but this is reserved for upcoming work.

5.1.4 Interpretation of the outer vortex tilt as a standing VRW pattern

The evidence presented above strongly suggests that the tilt evolution of the TC in our full physics experiment in the first 18–24 h is governed to zero order by a quasi-steady, slowly decaying wave number 1 VRW pattern. Figure 15a illustrates the low-level horizontal structure of this wave pattern at low levels above the BL. A strong dipole with an approximate N-S orientation is found in the inner core, representing the inner vortex tilt. A weaker dipole is found outside of the eyewall. This weaker, but more extensive dipole is associated with the tilt of the outer vortex[5]. It has been noted earlier (Jones, 1995, her Fig. 6a, here reproduced as Fig. 16b; Reasor et al., 2004, their Fig. 10) that the tilt of the outer part of the vortex can be significantly larger than that of the inner core. In our experiment the larger tilt of the outer vortex is readily visible in the vertical vorticity cross-section along the tilt axis in Fig. 16a.

The wave number 1 vorticity pattern in the shear cases is in stark contrast to the pattern in the no_shear case. In the no_shear case, outside the eyewall, the wave number 1 pattern is dominated frequently by a trailing spiral (Fig. 15b). Inspecting subsequent time steps (not shown, but qualitatively similar to Fig. 12) the spiral is found to propagate around the center. Outside of the spiral the vorticity anomalies are obviously not linked to a wave number 1 pattern. We regard the distinct differences between the wave number 1 characteristics in the no_shear and shear cases as further evidence that the wave number 1 asymmetry outside the eyewall in the shear cases is associated with the tilt of the outer vortex.

[5]The reverse sign of the vorticity dipole in the inner core is associated with a displacement of the vortex center in tilt direction.

ACPD
9, 10711–10775, 2009

5.2 Distribution of vertical motion outside of the eyewall

In this subsection we will present evidence that the convective asymmetry outside the eyewall is forced by the tilt of the outer TC-vortex. We will show that the downdrafts that flux low θ_e air into the BL are intimately connected to this convective asymmetry. The distribution of the downward flux of low θ_e on the vortex-scale is thus governed by balanced TC dynamics.

5.2.1 Ekman pumping by the outer-vortex-tilt vorticity anomaly

The vorticity rich region associated with the outer vortex tilt provides a favorable environment for the formation of updrafts outside of the eyewall. Vorticity anomalies within the BL produce frictional convergence and thus force upward motion. The vertical motion at the top of the BL due to this mechanism, w_{Ekman}, can be estimated from simple Ekman pumping theory:

$$w_{\text{Ekman}} = H_{\text{BL}}/2^{*}\zeta', \tag{25}$$

where ζ' denotes the vertical vorticity wave number 1 asymmetry at the top of the BL. H_{BL} denotes the height of the BL, set to 1.5 km. Chen and Yau (2001) used the Ekman pumping argument to show the coupling of propagating near-core VRWs with vertical motion. The wave number 1 perturbation of vertical motion and w_{Ekman} are compared at a representative time in Fig. 17. The structure and the magnitude of the vertical motion field can be explained to zero order by the simple Ekman pumping argument. Consistent with convective amplification of upward motion, the vertical motion asymmetry is stronger (by $\approx$ a factor of 2) compared to w_{Ekman}. The wave number 1 envelope of vertical motion – containing the convective asymmetry outside of the eyewall – can therefore be considered to be forced by the quasi-steady vorticity asymmetry associated with the tilt of the outer vortex.

ACPD
9, 10711–10775, 2009

5.2.2 Swirling of the updrafts and downdraft formation

The general vertical structure of the vertical motion outside of the eyewall (at 75 km radius) is illustrated in Fig. 18a. The updrafts are predominantly rooted in the BL downshear to downshear-right (between 250° and 330°). Due to advection by the swirling winds, ascent is along a slanted path[6]. The slope of θ_e isentropes – in particular the 360 K contour – indicates that air parcels rise almost pseudo-adiabatically. An extended region of downdrafts is found underneath and downwind of the updrafts, in the downshear-left to upshear quadrant of the storm. The downdrafts most likely form by evaporative cooling associated with falling rain, possibly enhanced by rain drag.

A pool of very low θ_e air is found between 140° and 180° below 4 km, extending into the BL. There is an indication that this pool is connected to the mid-level θ_e minimum between 5 km and 8 km suggesting that the low θ_e air originates from the mid-levels. Low-level θ_e values are frequently found to be smaller than the values of the mid-level minimum, in particular in the 20mps case (not shown). Non-pseudo-adiabatic processes, e.g. precipitative flux, may therefore play a role also. A strong azimuthal θ_e gradient is found between the region of updraft generation and the area where downdrafts reach the BL. At 1 km height the difference between the two regions at the time presented is 17 K.

The pattern of up- and downdrafts can be considerably more complex at some individual times. Regardless of fluctuations in the detailed structure, the general structure is persistent with time. This notion is supported by plotting the time average of the fields: all the features discussed above are still present in a 6 h average (Fig. 18b). This quasi-steadiness of the up- and downdraft pattern is an important difference to the no_shear case. Up- and downdraft couplets associated with wave number 1 VRWs are found in the no_shear case also (Fig. 19a); these "rain bands" propagate azimuthally

[6]The aspect ratio of the horizontal and vertical length scales is ≈20. Assuming an azimuthal wind speed of 50 ms^{-1} this yields an average vertical wind speed of 2.5 ms^{-1}, consistent with the values found in Fig. 18a.

ACPD
9, 10711–10775, 2009

and the associated downward flux of low θ_e is far less pronounced. As might be expected, in the time averaged sense the azimuthal structure is virtually homogeneous for the no_shear case (Fig. 19b). The quasi-steadiness of the convective pattern in the sheared cases indicates that the convection forms in response to a quasi-steady forcing, consistent with our hypothesis that the tilt of the outer vortex provides this forcing.

We speculate that the persistent location and the banded structure (cf. Fig. 11) of the updraft-downdraft couplet promote the pronounced BL θ_e depression in a Lagrangian sense. The basis for this speculation is that BL air parcels that spiral inward within the downdraft region experience a continuous frustration of the entropy uptake from the ocean surface. We further note that the persistent strong vertical gradient of θ_e at the top of the BL makes the intrusion of low θ_e air into the BL by downdrafts particularly effective. The existence of a pool of low θ_e air just above the BL also implies that air parcels do not need to descend from the mid-level minimum into the BL in a single downdraft plume to yield the observed θ_e depression.

6 An interpretation of storm recovery and shear evolution

In our experiments all storms re-intensify after the initial decrease in intensity. A comparison of the intensity and tilt magnitude time series show that the re-intensification in general coincides with the realignment of the TC. We argue that the reduction of the vortex tilt reduces the forcing of the convective asymmetry outside of the eyewall and thus hinders the formation of the quasi-stationary downdraft pattern. As the energy intake from the ocean surface is no longer considerably frustrated the storm is able to re-intensify.

The temporal evolution of the vertical wind shear somewhat complicates the interpretation of the recovery process. In a control experiment without a TC the vertical wind shear in thermal wind balance remains constant over the whole integration period. Due to the interaction with the TC, however, the shear magnitude and direction can be significantly modified (e.g. Wong and Chan, 2004). In the following we focus on

ACPD
9, 10711–10775, 2009

the evolution of the shear magnitude representative for the near-core region.

Vertical wind shear is calculated as the vector difference between the average horizontal winds on a disc around the storm center at 12 km and 1.5 km height, an approximation to the commonly used 200 hPa and 850 hPa levels. A disc with 120 km radius is used as this is the largest radius for which data from the innermost domain is available for all cases at all times[7].

First it is noted that a northerly shear component develops in the shear cases (not shown), consistent with the southward motion component (Fig. 6). This northerly shear can be attributed to the downshear displacement of the outflow anomaly (e.g. Wu and Emanuel, 1993).

The shear magnitude in the near-core region can reach 5–7 ms^{-1} even without environmental shear (Fig. 20). This illustrates that internal storm dynamics can project considerably on this shear measure. In the 20mps case the shear magnitude decreases considerably after the first 12 h. Subsequently, shear values range between 6 and 11 ms^{-1}. The pattern of shear evolution is similar in the 15mps case, with slightly smaller values than in the 20mps case. Shear values in the 10mps case range between 3 ms^{-1} and 11 ms^{-1} throughout the experiment with a peak of 16 ms^{-1} around 16 h.

The left-of-shear tilt equilibrium is considered an optimal configuration because the shear imposed by the vortex tilt opposes the environmental shear (e.g. Jones, 1995; Reasor et al., 2004). In our experiment the vortex settles in the left-of-shear equilibrium within the first 1–2 h after the shear is imposed, well before the decrease of shear magnitude. We do not find a considerable shear reduction in the first few hours of our experiment. It is possible that using a radial range of 120 km for the shear calculation underestimates the shear reduction in the inner core. It is obvious, however, that another mechanism is involved in the shear reduction in our 20mps and 15mps cases also.

[7]The TC in the 20mps case moves rather close to the boundary of the innermost domain at the end of the experiment.

ACPD
9, 10711–10775, 2009

We hypothesise that an intense TC is able to axisymmetrise the storm relative flow in the near-core environment to some degree. The shear that affects the core of the system is thus significantly reduced. It stands to reason that the storm can more completely re-align and thus re-intensify in the reduced-shear environment. It should be kept in mind that the shear flow in our experiment is only forced by the boundary conditions of the outer domain. We speculate that the ability of the vortex to reduce the near-core shear is less pronounced when the shear is associated with a dynamically strong weather system, e.g. a digging mid-level trough.

This brief discussion suggests that a strong TC is affected by much less shear than what is imposed on the synoptic scale. We hypothesise that it is the shear within the Lagrangian boundary of the storm that controls the inner core dynamics. The important question of what determines the region in which the TC actually "feels" the vertical shear will be addressed in upcoming work.

7 Observational support and further discussion on convective asymmetries

Before the final conclusions are presented, we support our new paradigm with observations of vertically sheared TCs in the real atmosphere. Some more discussion on the formation of the convective asymmetry outside of the eyewall is provided also.

7.1 Asymmetric convection and associated downdraft pattern in the real atmosphere

The convective asymmetry outside of the eyewall in our experiment is reminiscent of the stationary band complex (SBC) defined by Willoughby et al. (1984). These authors consider the relationship between the SBC and the low-level storm relative flow, not explicitly the relationship with vertical shear. They note, however, that low-level storm relative flow requires a difference between the environmental flow at the steering level, usually found at mid-levels, and the low-level flow, and thus vertical shear. The ori-

ACPD
9, 10711–10775, 2009

entation of the convective asymmetry with respect to the low-level storm relative flow in our experiment is consistent with the results of Willoughby et al. (1984), although care must be taken when comparing their radar reflectivity data with our model vertical motion. The observations provided in Willoughby et al. (1984) thus support our notion of asymmetric convective activity outside of the eyewall in sheared TCs. Ample further evidence of the formation of this convective asymmetry in the satellite representation of real TCs in vertical shear can be found in the literature, e.g. in Black et al. (2002, Hurricane Olivia (1994), their Fig. 14).

The formation of downdrafts and the associated thermodynamic impact on the BL in vertically sheared TCs has not been a focus of observational studies yet. Powell (1990, among others) has documented downdrafts and the associated modification of the BL θ_e distribution on the scale of individual rain bands. A widespread flooding of the BL with low θ_e air by persistent downdrafts has not been observed yet. Here we provide two observations that indicate the existence of persistent downdrafts in the downshear-left to upshear quadrant of real storms. In Hurricane Omar (2008) an arc cloud band propagating away from the storm center in the downshear-left to upshear quadrant is found in visible satellite imagery (Fig. 21). Arc cloud bands indicate persistent downdrafts. Halverson et al. (2006), although focusing on the upper-level warm core structure of Hurricane Erin (2001) in vertical shear, present a map of surface divergence (their Fig. 4, here reproduced as Fig. 22). A region of strong surface divergence is evident from the contiguous purple arc-like feature in Fig. 22, with an estimated length and width of $O(400\,\text{km}) \times O(50\,\text{km})$. Halverson et al. (2006) did not comment on this vortex-scale feature. The feature is found downwind of a region of convergence that supports a spiral-like convective asymmetry dominated by wave number 1. It was this convective asymmetry that was emphasised in Halverson et al. (2006). Divergence at the surface implies, by mass continuity, downward motion above. At this time the direction of the shear is approximately from the South. The orientation of the convective asymmetry and the adjacent band of downdrafts is as predicted by our new paradigm.

ACPD
9, 10711–10775, 2009

7.2 Formation of the convective asymmetry outside the eyewall

Willoughby et al. (1984) provide an appealing explanation for the formation of the convective asymmetry outside of the eyewall based on the idea of a Lagrangian boundary between the swirling winds of the vortex and the low-level storm relative flow. To the best of our knowledge, however, no attempt has been reported in the literature to support Willoughby et al.'s ideas with higher resolution data. In the present study, we provide a complementary explanation based on balanced vortex dynamics: the convective asymmetry is forced by the vorticity asymmetry associated with the tilt of the outer vortex. Asymmetric frictional forcing due to storm motion has been shown previously to also force convective asymmetries (Shapiro, 1983; Kepert, 2001; Kepert and Wang, 2001). In these studies the asymmetries due to storm motion appear to be confined to the inner core. Unpublished results by Ooyama (1986), however, indicate that frictionally forced asymmetries in the convergence pattern can extend outward to a radius of $O(100\,\mathrm{km})$. It seems therefore possible that asymmetric frictional forcing further modulates the convective asymmetry outside of the eyewall.

In all of these studies on asymmetric frictional forcing, the assumptions are made that the pressure distribution at the top of the BL is symmetric and that the developing asymmetries can be found as a stationary solution. It is not clear to us if these assumptions hold for a sheared, and thus inherently asymmetric TC undergoing pronounced intensity modification. An observational study by Corbosiero and Molinari (2003) does not support the idea that storm motion plays an important role for the structure of a TC in vertical shear. Using lightning data in 303 sample time periods of 35 TCs, Corbosiero and Molinari conclude that the distribution of asymmetric convection is governed by the direction of environmental shear rather than the motion vector, at least for moderate to strong shear values.

Clearly, more research is necessary to disentangle the individual contributions to the formation of what has been dubbed the "stationary band complex".

ACPD
9, 10711–10775, 2009

8 Conclusions

An important roadblock to improved intensity forecasts is our incomplete understanding of the interaction of a TC with the environmental flow. In this study we have thus revisited the problem of vertically sheared TCs in an idealised numerical experiment. A TC that was spun up in a quiescent environment is subjected to a unidirectional shear profile with cosine vertical structure. We considered moderate to strong shear values and an intense tropical cyclone. In all experiments the TC is resilient but significant differences in the intensity evolution occurred.

The evidence presented in this article points to an unsung pathway to intensity modification by vertical shear: vertical shear impacts the energy cycle of a TC at a critical part – the inflow layer of the storm. Flushing of low θ_e air into the BL outside of the eyewall significantly depresses BL θ_e values. The BL θ_e values do not recover sufficiently before reaching the eyewall, leading to lower θ_e values within the eyewall convection. This implies a frustration of the thermodynamic cycle of the TC heat engine. Less kinetic energy can be generated and a decrease in storm intensity is expected. The high correlation between the flushing of the BL with low θ_e air and the intensity evolution of the storm supports this hypothesis.

The downdrafts that flush the BL with low θ_e air are tied to a quasi-stationary convective asymmetry outside of the eyewall. The downdrafts form downwind and below the helical updrafts. The formation location indicates that evaporative cooling, possibly enhanced by precipitative drag, is the dominant downdraft formation mechanism. We argue that the quasi-steadiness of the updraft-downdraft pattern has an important implication for the efficiency of the downward flux of low θ_e air into the BL: underneath the persistent downdrafts a pool of low θ_e air builds up, yielding a strong vertical θ_e gradient at the top of the BL. Downdrafts within this region do not need to originate at the level of the tropospheric θ_e minimum to cause a significant depression of BL θ_e values.

We propose that the convective asymmetry outside of the eyewall is linked to the bal-

ACPD
9, 10711–10775, 2009

anced dynamics of the TC vortex subject to moderate to strong vertical shear. To zero order, the tilt evolution of the sheared TC in our full-physics experiment is governed by balanced dynamics. A heuristic argument is that the tilt evolution is consistent with predictions by the forced-damped model of Reasor et al. (2004). This model is based on vortex Rossby wave dynamics and assumes that the vortex tilt due to vertical shear strongly projects on wave number 1 asymmetries. The tilt of our vortex is indeed reasonably well represented by the (azimuthal) wave number 1 vorticity asymmetry. The fact that wave number 1 asymmetries dominate the total TC asymmetries in our shear experiments is further evidence for a balanced evolution. In the sense of AB theory (Shapiro and Montgomery, 1993) wave number 1 asymmetries can be approximately described as balanced. To our knowledge, this is the first publication that indicates a balanced behaviour of a TC vortex outside the inner core, out to radii of a few RMW, in a high-resolution full-physics model experiment. We dedicate a companion paper to further verify the dominant balanced nature of the vortex dynamics in that region. The tilt of the outer vortex in our experiments is considerably larger than the tilt of the eyewall, consistent with previous numerical experiments of dry vortices (Jones, 1995; Reasor et al., 2004). This outer-vortex tilt constitutes a wave number 1 vorticity asymmetry near the top of the BL outside of the eyewall out to ≈160 km radius. Vorticity anomalies within the BL produce frictional convergence and thus force upward motion. The positive vorticity anomaly associated with the wave number 1 pattern thus defines a preferred region of updraft formation. Consistent with results of Chen and Yau (2001), a simple Ekman pumping argument provides a zero order explanation for the associated wave number 1 vertical motion asymmetry. Convective feedback amplifies the updrafts and favors the smaller scales. Within the wave number 1 envelope the convection takes the form of bands and clusters.

In a modeling study like this, the formation of downdrafts might be sensitive to the background sounding and the microphysics parameterisation. Both sensitivities should be investigated in future numerical experiments. Using a more complex microphysics scheme – in particular including the ice phase – less intense downdrafts might be expected because ice particles fall out at much smaller velocity. Significant downdrafts,

ACPD
9, 10711–10775, 2009

however, appear to form in our experiment below the freezing level at 5–6 km (Fig. 18a). In conjunction with the observational support given in the previous paragraph, we thus believe that the downdraft formation and the associated significant BL θ_e depression is not an artifact of the warm rain scheme. We speculate that a potential sensitivity to the initial sounding has a physical meaning and might have important implications for intensity forecasts. The flushing of the BL with low θ_e air might be particularly pronounced when the asymmetric convection outside the eyewall interacts with anomalously dry low to mid-level air in the downshear-left semicircle. Observations of the thermodynamic properties of the environmental air in this region should prove helpful towards obtaining a more complete understanding of intensity change associated with vertical shear.

Acknowledgements. We appreciate collaboration with Kerry Emanuel (MIT). The first author enjoys support from an NRC Postdoctoral Award. This work is supported by NFS grants ATM-0649946 and ATM-0715426.

References

Bender, M. A.: The effect of relative flow on the asymmetric structure in the interior of hurricanes, J. Atmos. Sci., 54, 703–724, 1997. 10715, 10716

Black, M. L., Gamache, J. F., Marks, F. D., Samsury, C. E., and Willoughby, H. E.: Eastern Pacific Hurricanes Jimena of 1991 and Olivia of 1994: The effect of vertical shear on structure and intensity, Mon. Weather Rev., 130, 2291–2312, 2002. 10726, 10744

Black, P. G., D'Asaro, E. A., Drennan, W. M., French, J. R., Niiler, P. P., Sanford, T. B., Terrill, E. J., Walsh, E. J., and Zhang, J. A.: Air-sea exchange in hurricanes: Synthesis of observations from the Coupled Boundary Layer Air-Sea Transfer experiment, B. Am. Meteorol. Soc., 88, 357–374, 2007. 10721

Braun, S. A. and Wu, L.: A numerical study of Hurricane Erin (2001). Part II: Shear and the organization of eyewall vertical motion, Mon. Weather Rev., 135, 1179–1194, 2007. 10726

Braun, S. A., Montgomery, M. T., and Pu, Z.: High-resolution simulation of Hurricane Bonnie (1998). Part I: The organization of eyewall vertical motion, J. Atmos. Sci., 63, 19–42, 2006. 10715, 10726

Carr, L. E. and Williams, R. T.: Barotropic vortex stability to perturbations from axisymmetry, J. Atmos. Sci., 46, 3177–3191, 1989. 10716
Chen, Y. and Yau, M. K.: Spiral bands in a simulated hurricane. Part I: Vortex Rossby wave verification, J. Atmos. Sci., 58, 2128–2145, 2001. 10739, 10747
Clark, T. L. and Farley, R. D.: Severe downslope windstorm calculations in two and three spatial dimensions using anelastic interactive grid nesting: A possible mechanism for gustiness, J. Atmos. Sci., 41, 329–350, 1984. 10720
Corbosiero, K. L. and Molinari, J.: The relationship between storm motion, vertical wind shear, and convective asymmetries in tropical cyclones, J. Atmos. Sci., 60, 366–376, 2003. 10745
Cotton, W. R. and Coauthors: RAMS 2001: Current status and future directions, Meteorol. Atmos. Phys., 82, 5–29, 2003. 10717
Cram, T. A., Persing, J., Montgomery, M. T., and Braun, S. A.: A Lagrangian trajectory view on transport and mixing processes between the eye, eyewall, and environment using a high-resolution simulation of Hurricane Bonnie (1998), J. Atmos. Sci., 64, 1835–1856, 2007. 10716, 10730
Davis, C. A., Jones, S. C., and Riemer, M.: Hurricane vortex dynamics during Atlantic extratropical transition, J. Atmos. Sci., 65, 714–736, 2008. 10713, 10715
DeMaria, M.: The effect of vertical shear on tropical cyclone intensity change, J. Atmos. Sci., 53, 2076–2088, 1996. 10714
Emanuel, K. A.: An air-sea interaction theory for tropical cyclones. Part I: Steady-state maintenance, J. Atmos. Sci., 43, 585–605, 1986. 10715, 10753, 10754
Emanuel, K. A.: The theory of hurricanes, Annu. Rev. Fluid Mech., 23, 179–196, 1991. 10715
Frank, W. M. and Ritchie, E. A.: Effects of vertical wind shear on the intensity and structure of numerically simulated hurricanes, Mon. Weather Rev., 129, 2249–2269, 2001. 10715, 10716, 10726
Halverson, J. B., Simpson, J., Heymsfield, G., Pierce, H., Hock, T., and Ritchie, L.: Warm core structure of Hurricane Erin diagnosed from high altitude dropsondes during CAMEX-4, J. Atmos. Sci., 63, 309–324, 2006. 10744, 10775
Hill, G. E.: Factors controlling the size and spacing of cumulus clouds as revealed by numerical experiments, J. Atmos. Sci., 31, 646–673, 1974. 10717
Jones, S. C.: The evolution of vortices in vertical shear. I: Initially barotropic vortices, Q. J. Roy. Meteorol. Soc., 121, 821–851, 1995. 10713, 10738, 10742, 10747, 10769
Jones, S. C.: The evolution of vortices in vertical shear. III: Baroclinic vortices, Q. J. Roy.

Meteorol. Soc., 126, 3161–3185, 2000. 10714
Jordan, C. L.: Mean sounding for the West Indies area, J. Atmos. Sci., 15, 91–97, 1958. 10721
Kepert, J.: The dynamics of boundary layer jets within the tropical cyclone core. Part I: Linear theory, J. Atmos. Sci., 58, 2469–2484, 2001. 10745
Kepert, J. and Wang, Y.: The dynamics of boundary layer jets within the tropical cyclone core. Part II: Nonlinear enhancement, J. Atmos. Sci., 58, 2485–2501, 2001. 10745
Kessler, E.: On the distribution and continuity of water substance in atmospheric circulations, Meteor. Monogr., 32, Amer. Meteor. Soc., 1969. 10717
Klemp, J. B. and Wilhelmson, R. B.: The simulation of three-dimensional convective storm dynamics, J. Atmos. Sci., 35, 1070–1096, 1978. 10720
Lilly, D. K.: On the numerical simulation of buoyant convection, Tellus, 14, 148–172, 1962. 10717
Makarieva, A. M., Gorshkov, V. G., and Li, B.-L.: On the validity of representing hurricanes as Carnot heat engine, Atmos. Chem. Phys. Discuss., 8, 17423–17437, 2008, http://www.atmos-chem-phys-discuss.net/8/17423/2008/. 10715
Melander, M. V., McWilliams, J. C., and Zabusky, N. J.: Axisymmetrization and vorticity-gradient intensification of an isolated two-dimensional vortex through filamentation, J. Fluid Mech., 178, 137–159, 1987. 10716
Montgomery, M. T., Nguyen, S. V., Smith, R. K., and Pershing, J.: Do tropical cyclones intensify by WISHE?, Q. J. Roy. Meteorol. Soc., accepted, 2009. 10714
Nguyen, S. V., Smith, R. K., and Montgomery, M. T.: Tropical-cyclone intensification and predictability in three dimensions, Q. J. Roy. Meteorol. Soc., 134, 563–82, 2008. 10714
Ooyama, K. V.: A spectral prediction model on nested domains and its application to asymmetric flow in the hurricane boundary layer, in: International Symposium on Short and Medium Range Numerical Weather Prediction, WMO/IUGG, Tokyo, Japan, 1986. 10745
Pielke, R. A. and Coauthors: A comprehensive meteorological modeling system – RAMS, Meteor. Atmos. Phys., 49, 69–91, 1992. 10717
Powell, M. D.: Boundary layer structure and dynamics in outer hurricane rainbands. Part II: Downdraft modification and mixed layer recovery, Mon. Weather Rev., 118, 918–938, 1990. 10744
Reasor, P. D. and Montgomery, M. T.: Three-dimensional alignment and corotation of weak, TC-like vortices via linear vortex Rossby waves, J. Atmos. Sci., 58, 2306–2330, 2001. 10714
Reasor, P. D., Montgomery, M. T., and Grasso, L. D.: A new look at the problem of tropical

ACPD
9, 10711–10775, 2009

cyclones in vertical shear flow: Vortex resiliency, J. Atmos. Sci., 61, 3–22, 2004. 10713, 10735, 10736, 10738, 10742, 10747
Schecter, D. A. and Montgomery, M. T.: On the symmetrization rate of an intense geophysical vortex, Dynam. Atmos. Oceans, 37, 55–88, 2003. 10713
Schecter, D. A. and Montgomery, M. T.: Waves in a cloudy vortex, J. Atmos. Sci., 64, 314–337, 2007. 10713, 10735
Schubert, W. H., Montgomery, M. T., Taft, R. K., Guinn, T. A., Fulton, S. R., Kossin, J. P., and Edwards, J. P.: Polygonal eyewalls, asymmetric eye contraction, and potential vorticity mixing in hurricanes, J. Atmos. Sci., 56, 1197–1223, 1999. 10724
Shapiro, L. J.: The asymmetric boundary layer flow under a translating hurricane, J. Atmos. Sci., 40, 1984–1998, 1983. 10745
Shapiro, L. J. and Montgomery, M. T.: A three-dimensional balance theory for rapidly rotating vortices, J. Atmos. Sci., 50, 3322–3335, 1993. 10737, 10747
Simpson, R. H. and Riehl, H.: Mid-tropospheric ventilation as a constraint on hurricane development and maintenance, in: Proc. Tech. Conf. on Hurricanes, Amer. Meteor. Soc., Miami, FL, D4.1–D4.10, 1958. 10715
Smagorinsky, J.: General circulation experiments with the primitive equations, Mon. Weather Rev., 91, 99–164, 1963. 10717
Smith, R. K., Ulrich, W., and Sneddon, G.: On the dynamics of hurricane-like vortices in vertical-shear flows, Q. J. Roy. Meteorol. Soc., 126, 2653–2670, 2000. 10713
Smith, R. K., Montgomery, M. T., and Vogl, S.: A critique of Emanuel's hurricane model and potential intensity theory, Q. J. Roy. Meteorol. Soc., 134, 551–561, 2008. 10715
Tripoli, G. J. and Cotton, W. R.: The use of ice-liquid water potential temperature as a thermodynamic variable in deep atmospheric models, Mon. Weather Rev., 109, 1094–1102, 1981. 10717
Vecchi, G. A. and Soden, B. J.: Increased tropical Atlantic wind shear in model projections of global warming, Geophys. Res. Lett., 34, L08702, doi:10.1029/2006GL028905, 2007. 10713
Wang, Y., Montgomery, M., and Wang, B.: How much vertical shear can a well-developed tropical cyclone resist?, in: Preprints of the 26th Conference on Hurricanes and Tropical Meteorology, Amer. Meteor. Soc., Miami, FL, 100–101, 2004. 10726
Willoughby, H. E., Marks, F. D., and Feinberg, R. J.: Stationary and moving convective bands in hurricanes, J. Atmos. Sci., 41, 3189–3211, 1984. 10743, 10744, 10745
Wong, M. L. M. and Chan, J. C. L.: Tropical cyclone intensity in vertical wind shear, J. Atmos.

Sci., 61, 1859–1876, 2004. 10714, 10716, 10741
Wu, C.-C. and Emanuel, K. A.: Interaction of a baroclinic vortex with background shear: Application to hurricane movement, J. Atmos. Sci., 50, 62–76, 1993. 10742
Wu, L. and Braun, S. A.: Effects of environmentally induced asymmetries on hurricane intensity: A numerical study, J. Atmos. Sci., 61, 3065–3081, 2004. 10714
Zhang, J. A., Black, P. G., French, J. R., and Drennan, W. M.: First direct measurements of enthalpy flux in the hurricane boundary layer: The CBLAST results, Geophys. Res. Lett., 35, L14813, doi:10.1029/2008GL034374, 2008. 10721

ACPD
9, 10711–10775, 2009

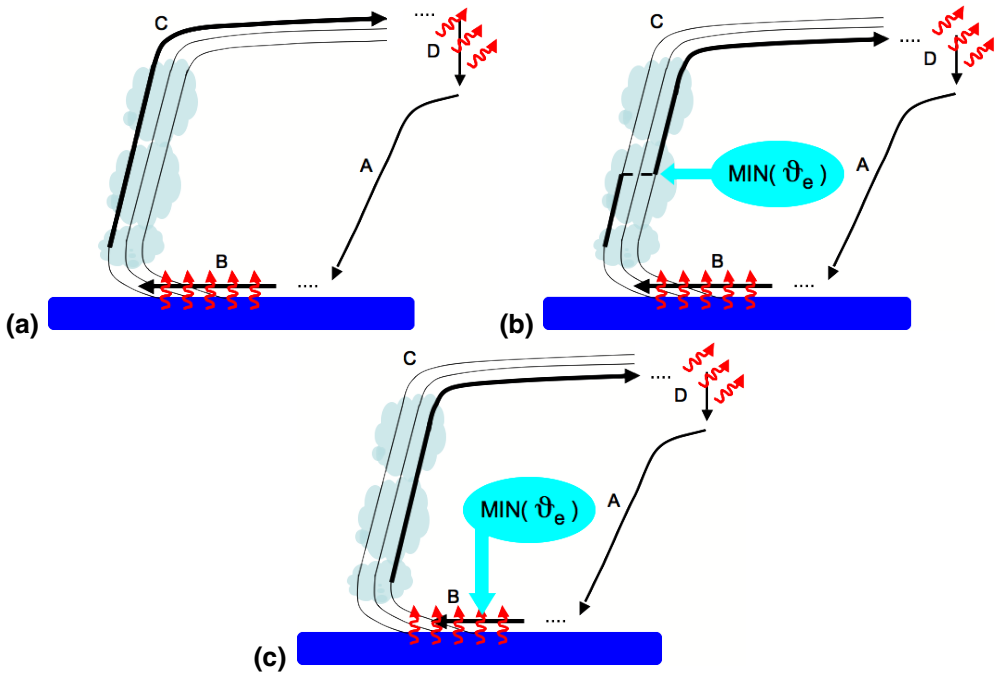

Fig. 1. Schematic of Emanuel's axisymmetric, steady-state model of a TC working as a Carnot cycle heat engine and two hypothesised impacts of vertical shear on the thermodynamic cycle. The storm center is to the left in each figure and the blue region indicates the ocean. Black arrows denote the hypothesised path of air parcels and contours depict isentropes of θ_e, decreasing outward from the storm center. Curved red arrows indicate processes that change the moist entropy (i.e. θ_e) of an air parcel. **(a)** The undiluted Carnot cycle: air parcels take up heat from the ocean surface along the inflow leg B. The process is supposed to be isothermal. Then, the air parcels are supposed to rise moist-adiabatically in the eyewall and flare outward at upper level C. To close the thermodynamical cycle the air parcels are assumed to lose enough heat through radiative cooling to return to their ambient θ_e (D and A, see Emanuel, 1986). **(b)** Illustration of the effect of mid-level ventilation on the Carnot cycle. Low θ_e from the climatological mid-level minimum is assumed to be transported to and mixed with the air rising in the eyewall on a direct pathway, diluting eyewall θ_e values. Above the level of mixing the air parcel rise on a lower isentrope. **(c)** Illustration of the pathway proposed in this paper: downdrafts flush the near-core BL with low θ_e originating at mid-levels and thus quench the energy source of the storm in the inflow layer. Surface fluxes do not fully recover BL θ_e values and air parcels start rising at the base of the eyewall on a lower isentrope. Both processes (b) and (c) can work concurrently.

ACPD
9, 10711–10775, 2009

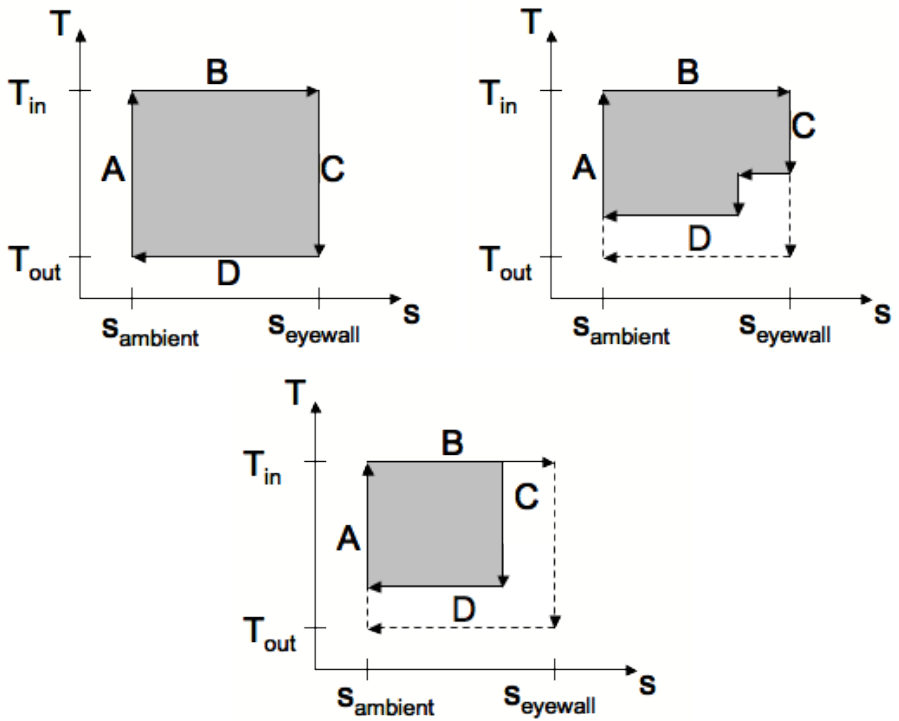

Fig. 2. Schematic temperature (T) – entropy (s) diagrams for the thermodynamic cycles depicted in Fig. 1. T_{in} and T_{out} denote the temperature of the inflow and outflow layer, respectively, and $s_{ambient}$ and $s_{eyewall}$ denote the moist entropy of ambient air and in the eyewall, respectively. The shaded area displays the work that is done by the Carnot cycle and that is assumed to be transformed into kinetic energy. This area is thus an estimate for the intensity of the TC that can be expected on the grounds of Emanuel's steady-state intensity theory. **(a)** the undiluted cycle, **(b)** effect of mid-level ventilation, and **(c)** flushing of the near-core BL with low θ_e air. The diagrams are reproduced from Brian Tang's PhD thesis proposal at MIT with permission.

ACPD
9, 10711–10775, 2009

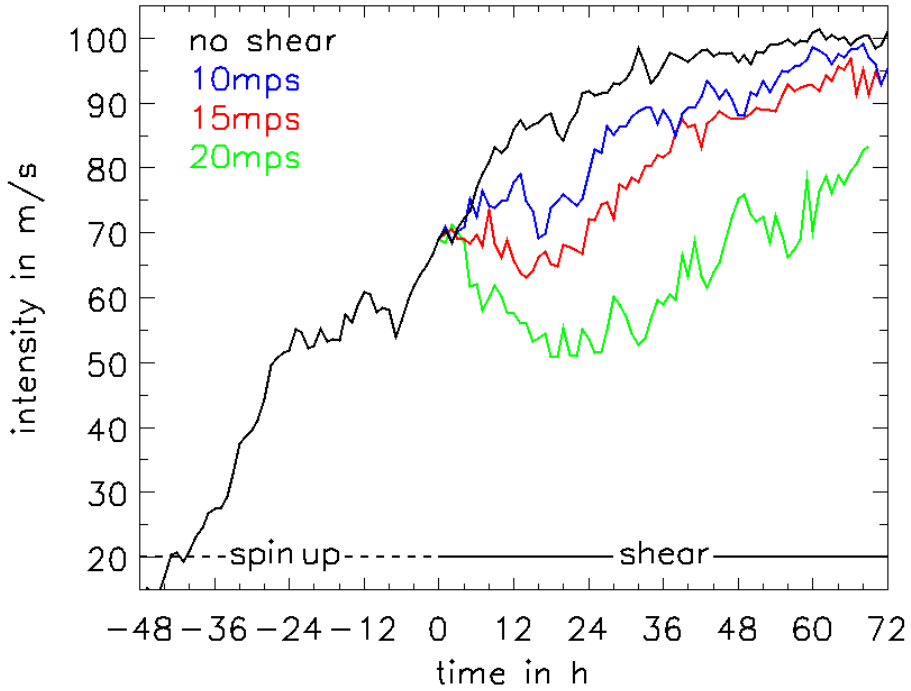

Fig. 3. Intensity time series for the spin up period (−48 h–0 h) and the respective shear experiments. Shear is imposed at 0 h.

ACPD
9, 10711–10775, 2009

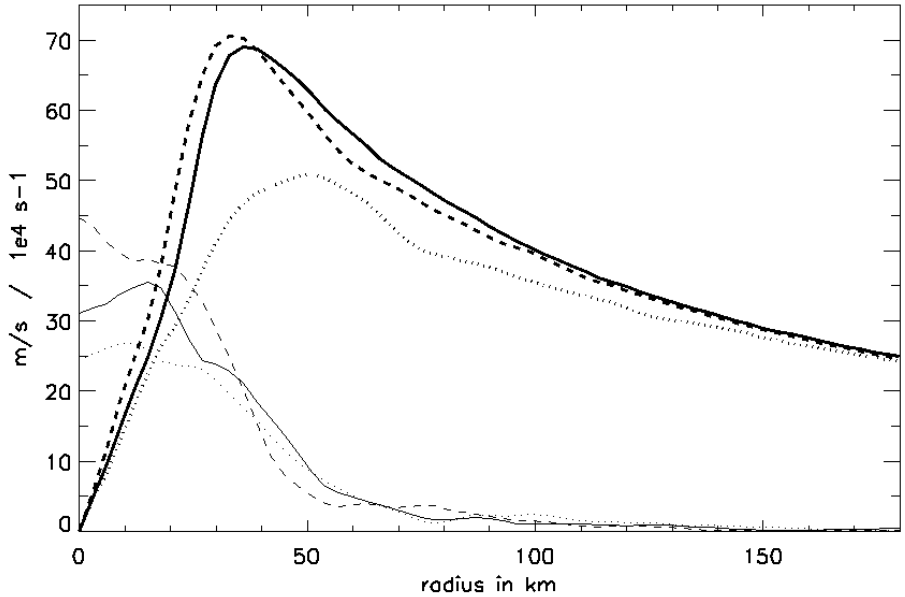

Fig. 4. Radial profiles of azimuthally averaged vorticity above the BL at 2 km height (thin) and tangential wind speed at 1 km height (thick) at time 0 h (solid), at 2 h (dashed) and at 18 h (dotted) for the 20mps case.

ACPD
9, 10711–10775, 2009

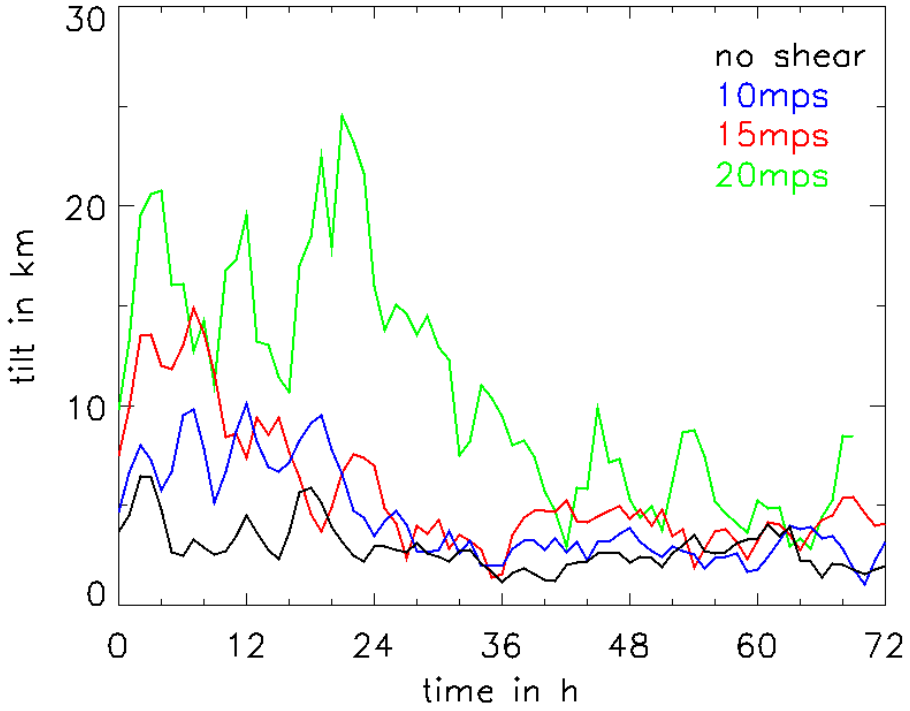

Fig. 5. Magnitude of vortex tilt for the no_shear (black), 10mps (blue), 15mps (red), and 20mps case (green), respectively. For clarity, the 3 h running mean of the time series is shown.

ACPD
9, 10711–10775, 2009

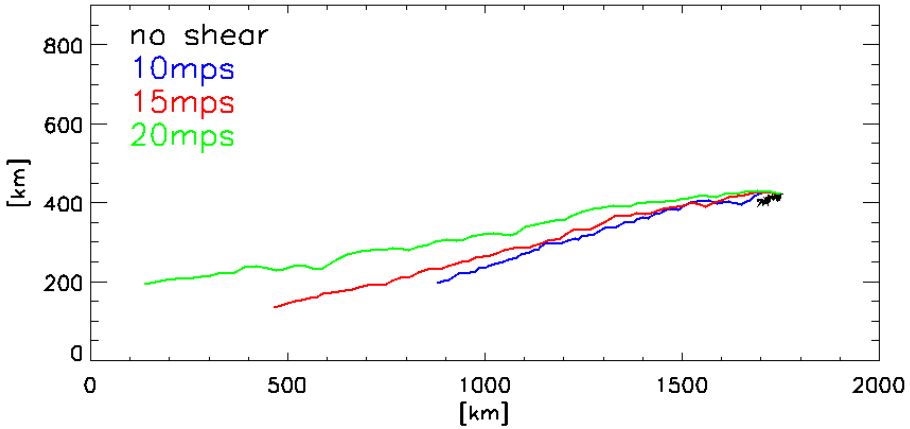

Fig. 6. TC tracks for the 20mps (green), 15mps (red), 10mps (blue) and the no_shear case (black) in the innermost model domain for the shear period from 0–72 h (69 h for 20mps due to proximity to the domain boundary).

ACPD
9, 10711–10775, 2009

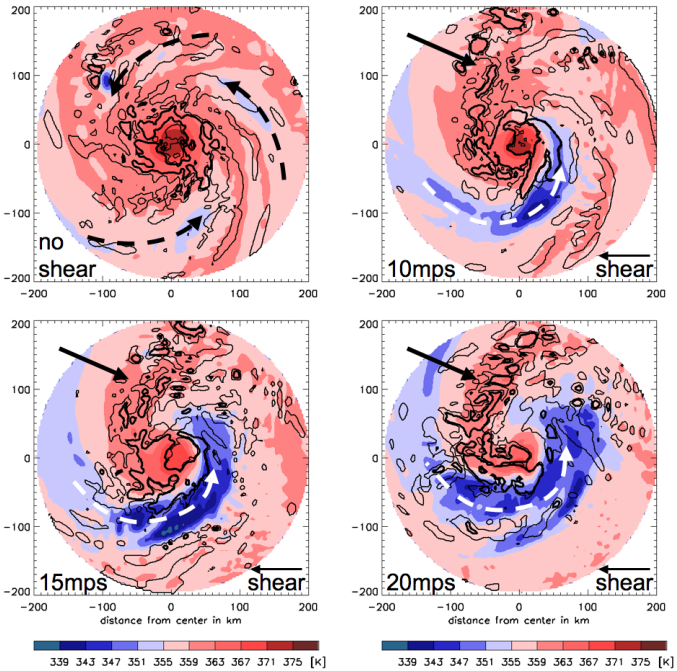

Fig. 7. Boundary layer θ_e (color, averaged over the lowest 1 km), and upward motion (thin contour: 0.2 ms^{-1}, thick contour: 1 ms^{-1}, averaged between 1.25 and 2 km height) at 5 h. The center of the TC is in the middle of the domain. The no_shear case is depicted in **(a)**, the 10mps, 15mps, and 20mps case in **(b)**, **(c)**, and **(d)**, respectively. The shear direction is indicated in the lower right corner of each plot. Solid arrows highlight the quasi-stationary convective asymmetry outside of the eyewall in the shear cases and dashed white arrows the quasi-stationary region of depressed BL θ_e air. The dashed black arrows indicate transient bands of somewhat reduced θ_e values in the no_shear case. The depicted times are representative for the early part of the experiments (see text for details).

ACPD
9, 10711–10775, 2009

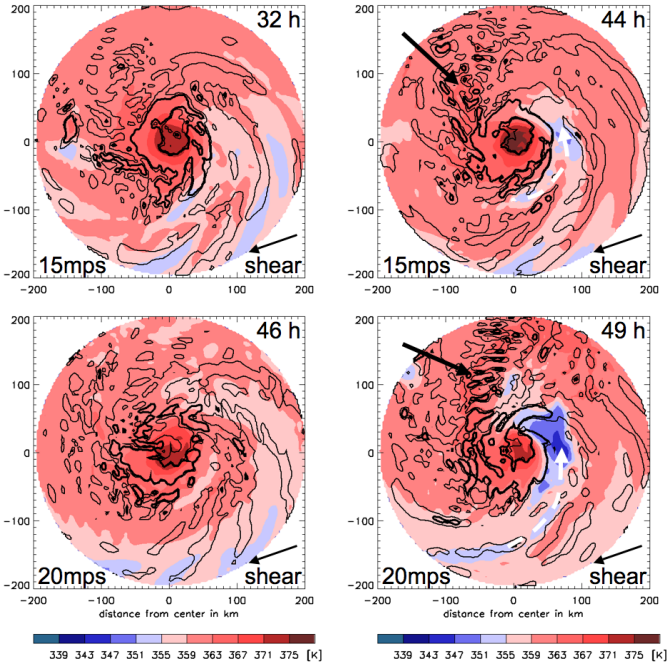

Fig. 8. Same as Fig. 7, but for the 15mps case (top row) at times 32 h **(a)**, and 44 h **(b)** and for the 20mps case (bottom row) at times 46 h **(c)**, 49 h **(d)**.

ACPD
9, 10711–10775, 2009

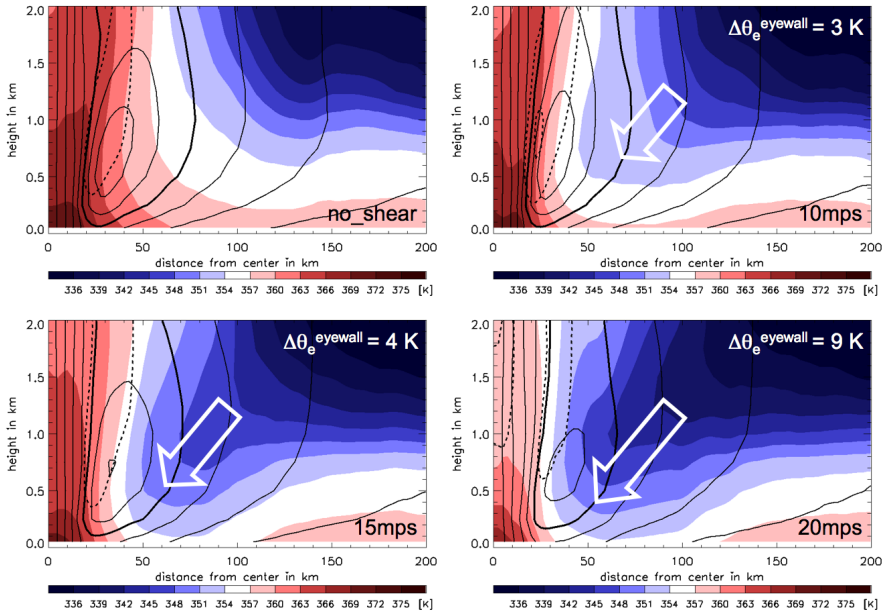

Fig. 9. Azimuthal mean of θ_e (color), tangential wind (solid contours, every 10 ms^{-1}, 50 ms^{-1} thick), and vertical motion (dashed, every 1 ms^{-1}) displayed in a height-radius format for the no_shear **(a)**, 10mps **(b)**, 15mps **(c)**, and 20mps case **(d)** at 5 h, representative for the early part of the experiments (see text for details).

ACPD
9, 10711–10775, 2009

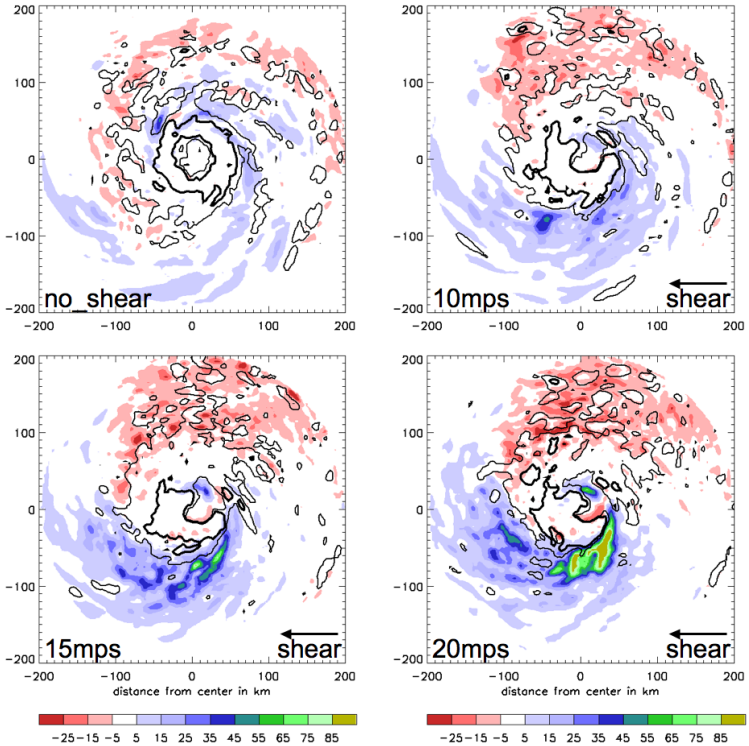

Fig. 10. Same as Fig. 7, but for the downward flux of θ'_e, DFX (color, in 0.1 K ms^{-1}), at the top of the inflow layer, defined as 1.5 km, averaged from 1 h to 6 h. The no_shear case is depicted in **(a)**, the 10mps, 15mps, and 20mps cases are depicted in **(b)**, **(c)**, and **(d)**, respectively.

ACPD
9, 10711–10775, 2009

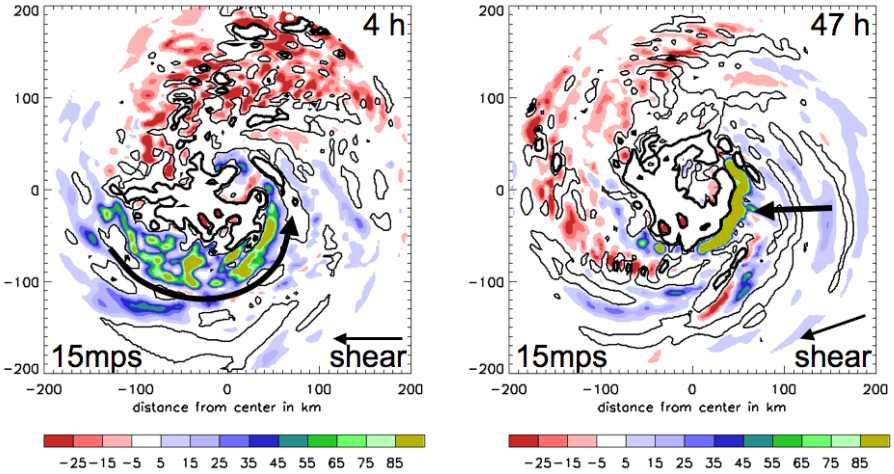

Fig. 11. Same as Fig. 10, but for the 15mps case at times 4 h **(a)** and 47 h **(b)**. The thick black arrows highlight the characteristic structure of DFX at the respective time.

ACPD
9, 10711–10775, 2009

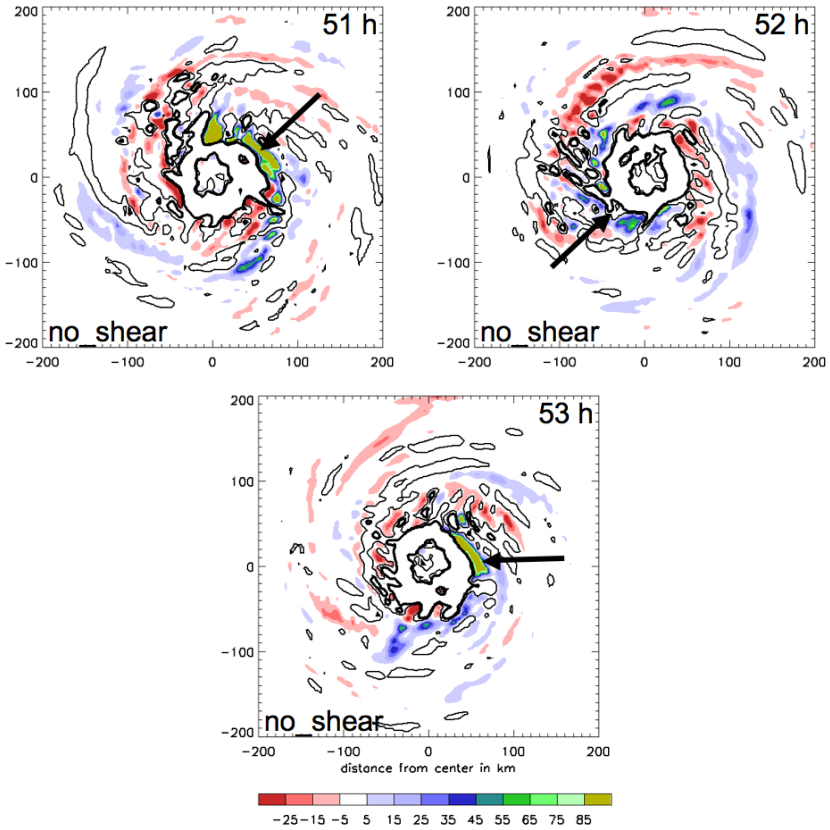

Fig. 12. Same as Fig. 10, but for the no_shear case at 3 consecutive hours – 51 h **(a)**, 52 h **(b)**, and 53 h, **(c)**.

ACPD
9, 10711–10775, 2009

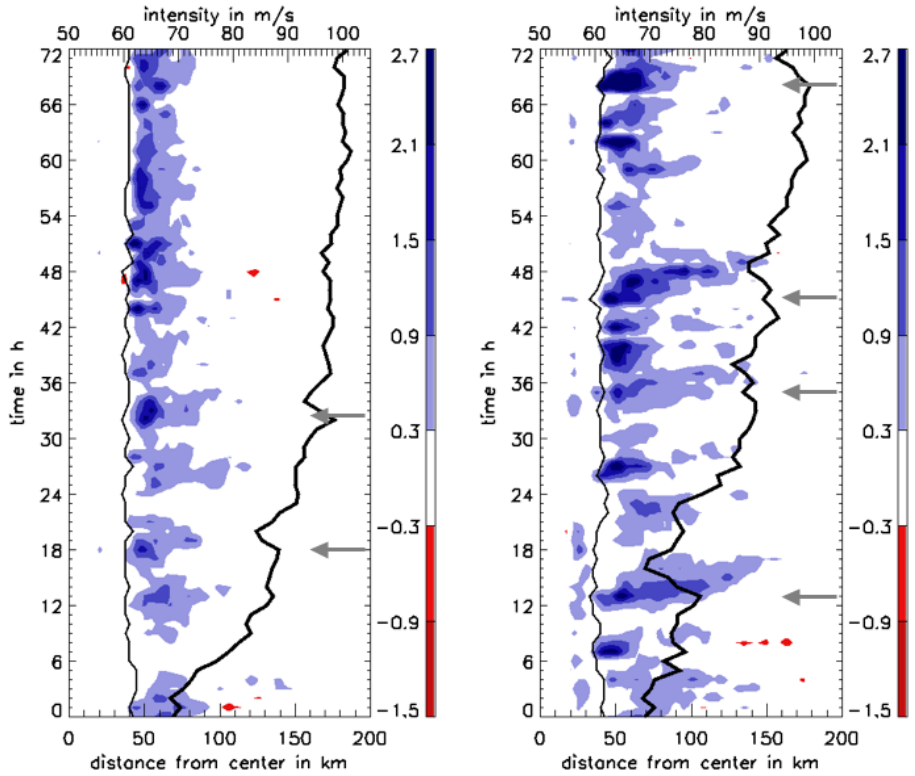

Fig. 13. Radial-time plot of the azimuthal average of downward flux of θ_e ($\overline{\text{DFX}}$, see text for definition) at 1.5 km height (color, in K ms^{-1}), time series of intensity (thick contour, scale at the top of the figures) and RMW (thin contour). The no_shear case is depicted in **(a)**, the 10mps, 15mps, and 20mps case in **(b)**, **(c)**, and **(d)**, respectively. Light gray arrows highlight DFX events that frustrate the re-intensification of the storm.

ACPD
9, 10711–10775, 2009

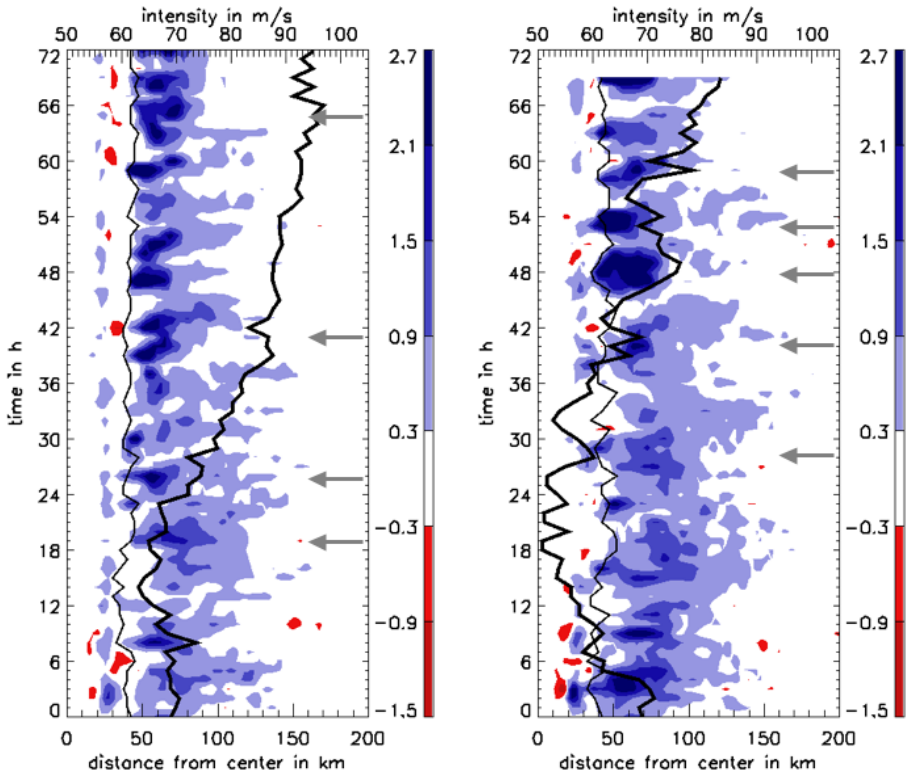

Fig. 13. Continued.

ACPD
9, 10711–10775, 2009

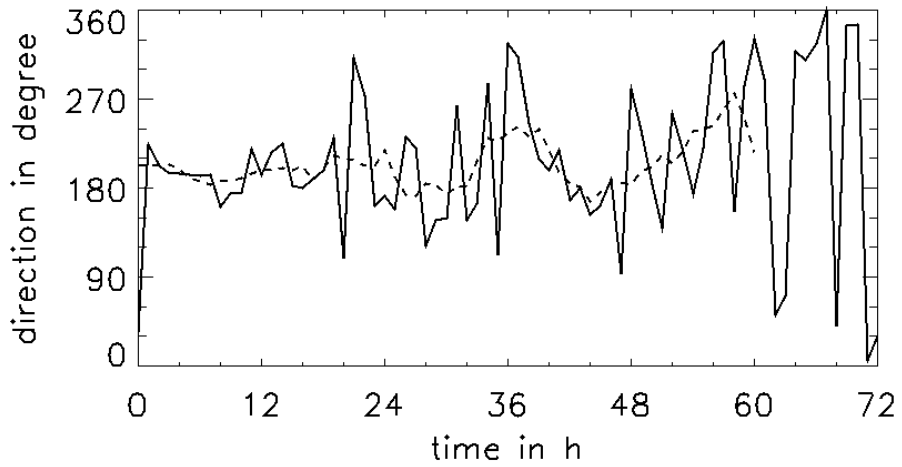

Fig. 14. Direction of tilt with height (solid) for the 15mps case (0° and 360°=North, 90°=East, 180°=South, and 270°=West). Tilt is calculated as the vector difference between the vorticity centroids at 10 km and 1 km. The 6 h running mean (dashed) is shown up to 60 h also. Later in the experiment, it is not clear if the TC vortex precesses with high frequency or oscillates around a predominant northerly direction. The averaged time series is thus shown until 60 h only.

ACPD
9, 10711–10775, 2009

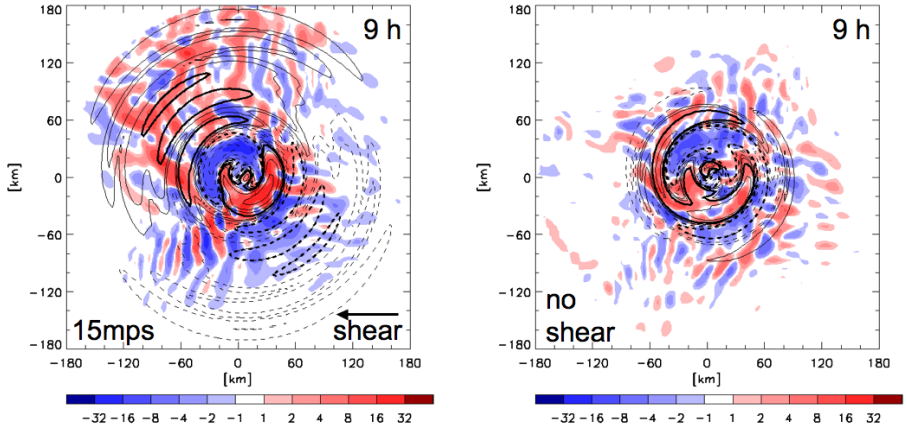

Fig. 15. Total (color, in 10^{-4} s^{-1}) and wave number 1 asymmetry (contour, half the color scale) of vorticity above the BL at 2 km height at a representative time (9 h) for the 15mps **(a)** and the no_shear **(b)** case. For the sheared case, most of the asymmetries reside inside the wave number 1 envelope out to large radii.

ACPD
9, 10711–10775, 2009

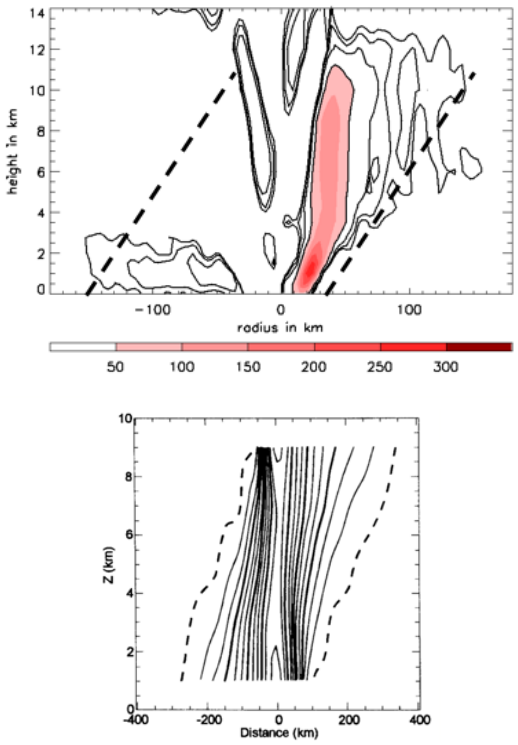

Fig. 16. **(a)** Vertical cross-section of positive, azimuthal wave number 1 vorticity asymmetry along the tilt axis oriented approximately North (left) to South (right), averaged from 2 h to 7 h. The color shaded region depicts the large asymmetry associated with the tilt of the inner core (color scale is in $10^{-5}s^{-1}$). Contours depict smaller values associated with the tilt of the outer vortex and are drawn at 5, 10, 20, and $50\times10^{-5}s^{-1}$. **(b)** Figure 6a from Jones (1995): a vertical cross section of vorticity along the tilt axis of a vortex in a dry primitive equation numerical experiment. The inner core is virtually aligned while the outer core region exhibits a significant tilt (note the different aspect ratio).

ACPD
9, 10711–10775, 2009

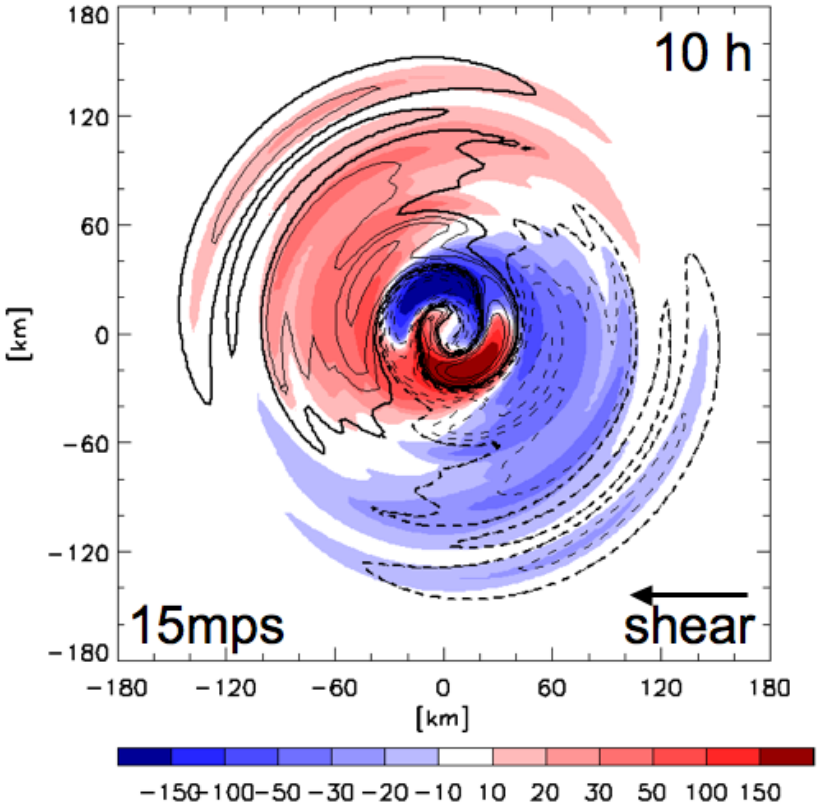

Fig. 17. Wave number 1 asymmetry of vertical motion (color, in cm s^{-1}) and w_{Ekman} at 1.5 km (contours, see text for definition) at a representative time (10 h). Contours are drawn at half the scale of the color bar, negative values are dashed. The ±5 cm s^{-1} contour is highlighted.

ACPD
9, 10711–10775, 2009

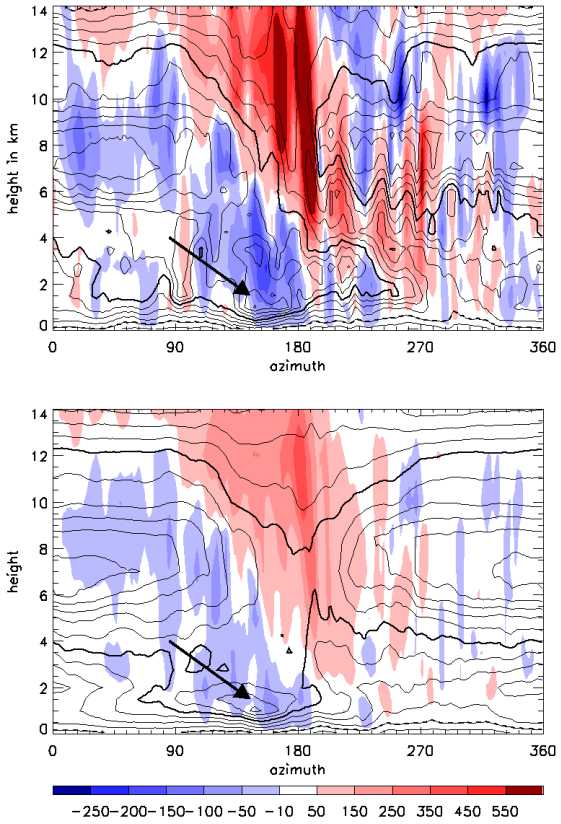

Fig. 18. Azimuth-height cross-section along radius 75 km of vertical motion (color, in cm s^{-1}) and θ_e (contours, every 2.5 K, 350 K thick, 360 K dashed) for the 15mps case. Looking South from the storm center, 90° is East and 270° is West. A snapshot at time 9 h is shown in **(a)**, a 6 h-average (7 h–12 h) is depicted in **(b)**. The arrow highlights low θ_e values associated with the downdraft pattern.

ACPD
9, 10711–10775, 2009

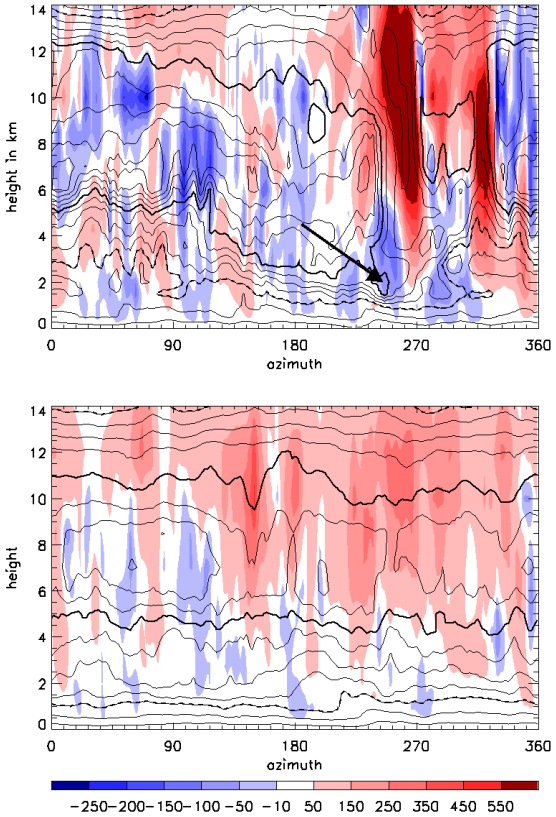

Fig. 19. Same as Fig. 18, but for the no_shear case.

ACPD
9, 10711–10775, 2009

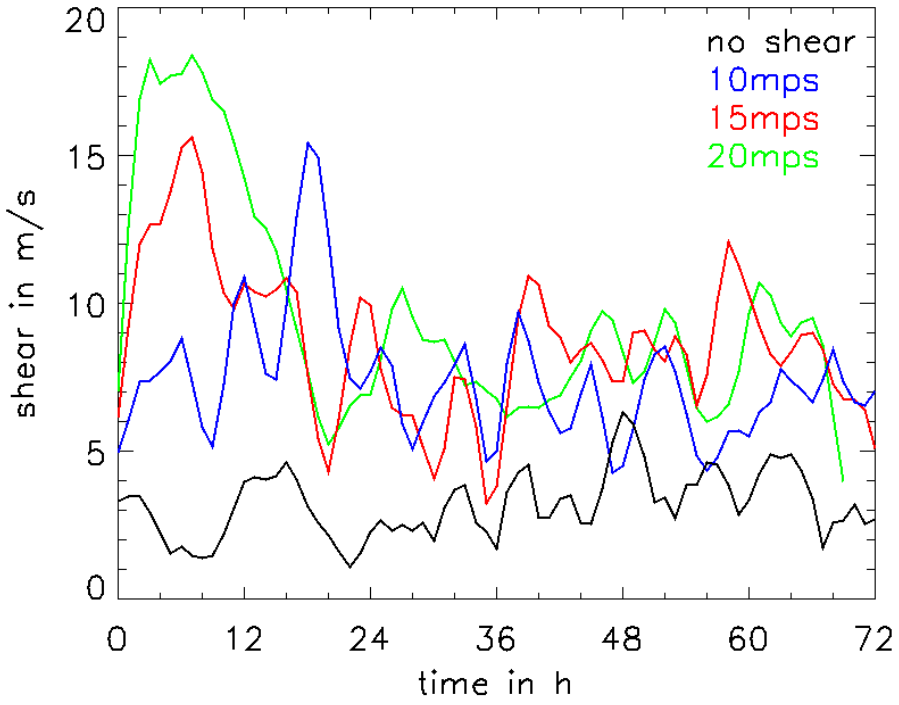

Fig. 20. Magnitude of the near-core shear for the no_shear (black), 10mps (blue), 15mps (red), and 20mps (green) case. Shear is calculated as the vector difference between the horizontal wind at 12 km and 1.5 km height, averaged horizontally over a disc around the storm center with a radius of 120 km. For clarity, the 3 h running mean of the time series is shown.

ACPD
9, 10711–10775, 2009

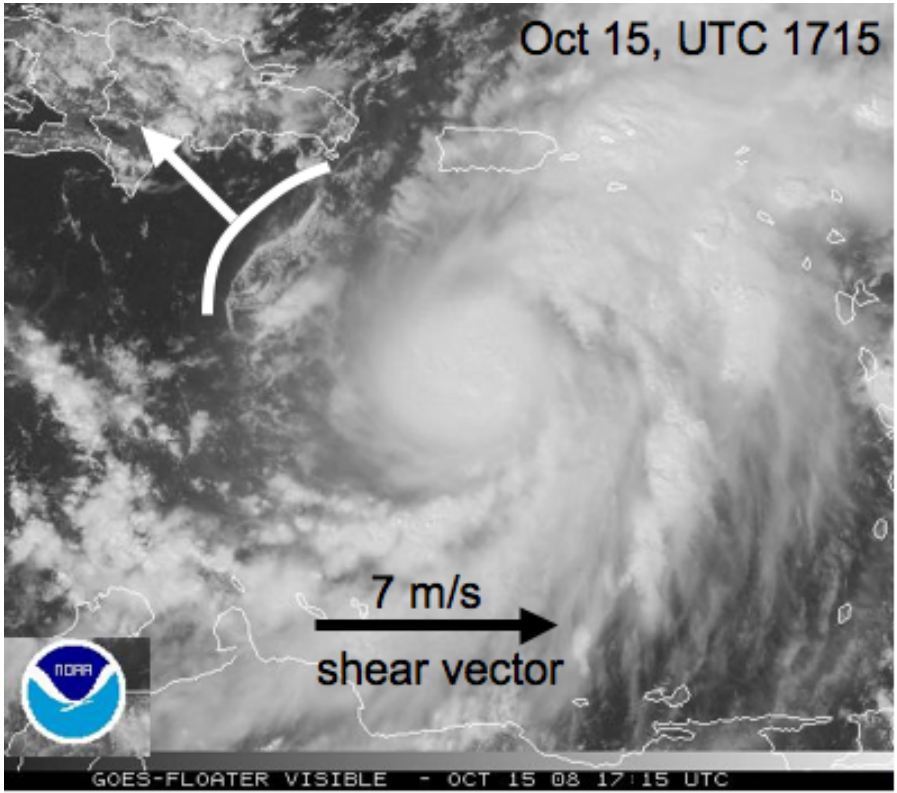

Fig. 21. Visible satellite imagery of Hurricane Omar south of Puerto Rico on 15 October 2008 at 17:15 UTC (courtesy of NOAA). The shear direction is from the West. Shear direction and magnitude are estimated from Chris Velden's *email shear product* at CIMMS (Velden, personal communication). The arc cloud band to the Northwest of the storm is highlighted by the white curve. The white arrow indicates the movement of the band relative to the storm center.

ACPD
9, 10711–10775, 2009

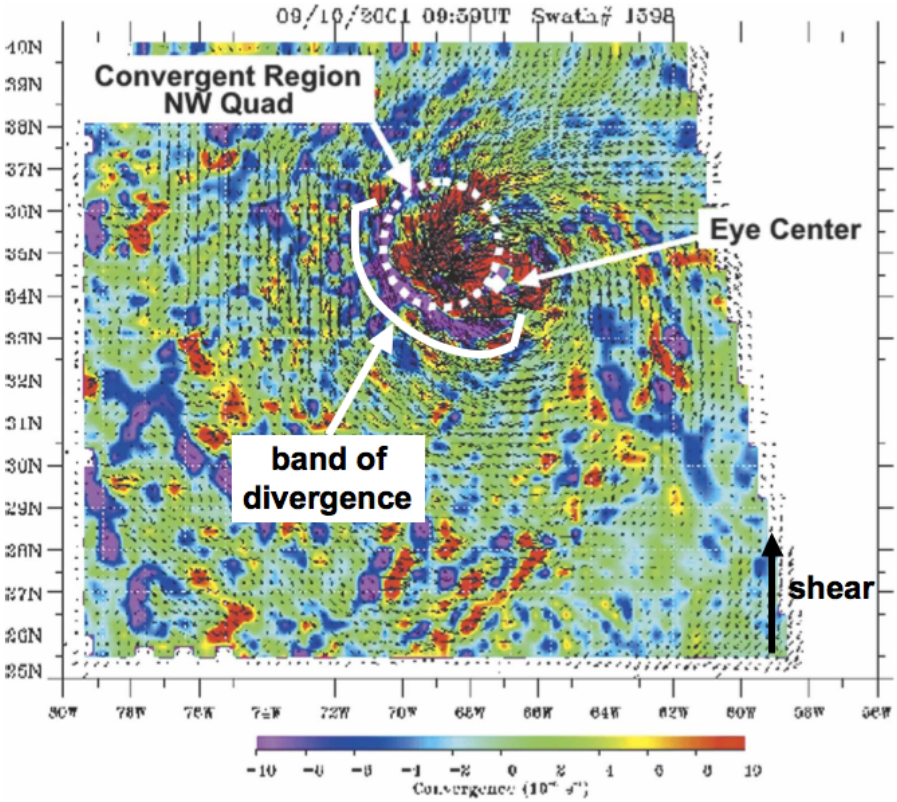

Fig. 22. Figure 4 from Halverson et al. (2006): convergence at sea level (color) and storm relative motion (arrows) for Hurricane Erin (2001) at 10:00 UTC 10 September, obtained from gridded QuickSCAT data. Red areas denote convergence, and purple show divergence. The authors of the present study have highlighted the band of divergence and indicated the approximate shear direction at this time. See comment in Halverson et al. (2006) about potential impact of rain contamination.

ACPD
9, 10711–10775, 2009